

LISA Galactic binaries with astrometry from Gaia DR3

THOMAS KUPFER ^{1,2} VALERIYA KOROL ^{3,4}

BOTH AUTHORS CONTRIBUTED EQUALLY TO THIS WORK

TYSON B. LITTENBERG,⁵ SWETA SHAH ^{6,7} ETIENNE SAVALLE ^{8,9} PAUL J. GROOT,^{10,11,12} THOMAS R. MARSH ¹³
MAUDE LE JEUNE,⁸ GIJS NELEMANS,^{10,14,15} ANNA F. PALA ¹⁶ ANTOINE PETITEAU ^{8,9} GAVIN RAMSAY ¹⁷
DANNY STEEGHS ¹³ STANISLAV BABAK,⁸

¹Hamburger Sternwarte, University of Hamburg, Gojenbergsweg 112, 21029 Hamburg, Germany

²Department of Physics and Astronomy, Texas Tech University, PO Box 41051, Lubbock, TX 79409, USA

³Max-Planck-Institut für Astrophysik, Karl-Schwarzschild-Straße 1, 85741 Garching, Germany

⁴Institute for Gravitational Wave Astronomy, School of Physics and Astronomy, University of Birmingham, Birmingham, B15 2TT, UK

⁵NASA Marshall Space Flight Center, Huntsville, Alabama 35811, USA

⁶Max Planck Institute for Gravitational Physics (Albert Einstein Institute), Callinstrasse 38, 30167 Hannover, Germany

⁷Leibniz Universität Hannover, Institut für Gravitationsphysik, Callinstrasse 38, 30167 Hannover, Germany

⁸Université de Paris, CNRS, Astroparticule et Cosmologie, 75013 Paris, France

⁹IRFU, CEA, Université Paris-Saclay, F-91191, Gif-sur-Yvette, France

¹⁰Department of Astrophysics/IMAPP, Radboud University, P.O.Box 9010, 6500 GL Nijmegen, The Netherlands

¹¹South African Astronomical Observatory, PO Box 9, Observatory, 7935, Cape Town, South Africa

¹²Department of Astronomy & Inter-University Institute for Data Intensive Astronomy, University of Cape Town, Private Bag X3, 7701 Rondebosch, South Africa

¹³Department of Physics, University of Warwick, Gibbet Hill Road, Coventry CV4 7AL, UK

¹⁴SRON, Netherlands Institute for Space Research, Niels Bohrweg 4, 2333 CA Leiden, The Netherlands

¹⁵Institute of Astronomy, KU Leuven, Celestijnenlaan 200D, B-3001 Leuven, Belgium

¹⁶European Space Agency, European Space Astronomy Centre, Camino Bajo del Castillo s/n, 28692 Villanueva de la Cañada, Madrid, Spain

¹⁷Armagh Observatory and Planetarium, College Hill, Armagh BT61 9DG, UK

ABSTRACT

Galactic compact binaries with orbital periods shorter than a few hours emit detectable gravitational waves at low frequencies. Their gravitational wave signals can be detected with the future *Laser Interferometer Space Antenna* (*LISA*). Crucially, they may be useful in the early months of the mission operation in helping to validate *LISA*'s performance in comparison to pre-launch expectations. We present an updated list of 55 candidate *LISA* detectable binaries with measured properties, for which we derive distances based on *Gaia* Data release 3 astrometry. Based on the known properties from EM observations, we predict the *LISA* detectability after 1, 3, 6, and 48 months using Bayesian analysis methods. We distinguish between verification and detectable binaries as being detectable after 3 and 48 months respectively. We find 18 verification binaries and 22 detectable sources, which triples the number of known *LISA* binaries over the last few years. These include detached double white dwarfs, AMCVn binaries, one ultracompact X-ray binary and two hot subdwarf binaries. We find that across this sample the gravitational wave amplitude is expected to be measured to $\approx 10\%$ on average, while the inclination is expected to be determined with $\approx 15^\circ$ precision. For detectable binaries these average errors increase to $\approx 50\%$ and to $\approx 40^\circ$ respectively.

Keywords: White dwarf stars (1799) — Compact binary stars (283) — Semi-detached binary stars (1443) — Gravitational wave sources (677)

1. INTRODUCTION

Binary systems composed of degenerate stellar remnants (white dwarfs, neutron stars and black holes) in orbits with periods of less than a few hours are predicted to be strong gravitational wave (GW) sources in our own Galaxy. A number of these systems – primarily consisting of a neutron star or white dwarf paired with a compact helium-star, white dwarf, or another neutron star – have been identified primarily through the observation in optical and X-ray electromagnetic (EM) wavebands. Some of these systems display remarkably short orbital periods, down to just several minutes (e.g. [Amaro-Seoane et al. 2023](#)). Binaries in a such a tight orbit emit GWs at mHz frequencies that can be detected directly with the future *Laser Interferometer Space Antenna* (*LISA*, [Amaro-Seoane et al. 2017](#)), and other future planned space-based GW observatories such as *TianQin* ([Luo et al. 2016](#); [Huang et al. 2020](#)), *Taiji* ([Ruan et al. 2018](#)) and the *Lunar Gravitational Wave Antenna* ([Harms et al. 2021](#)).

In this study we focus on the *LISA* mission, which is a European Space Agency (ESA)-led GW observatory currently scheduled for launch in the mid-2030s¹. Designed to operate in the frequency band between 0.1 mHz and 100 mHz ([Amaro-Seoane et al. 2017](#)), *LISA* is an ideal tool for discovering massive black hole mergers and extreme-/intermediate-mass ratio inspirals. In addition, it can survey the shortest period stellar remnant binaries throughout the entire Milky Way, providing a complementary view of our Galaxy to EM surveys (for a review see [Amaro-Seoane et al. 2023](#)). Both theory- and observation-based studies find that *LISA* will deliver a sample of $\mathcal{O}(10^4)$ binaries with orbital periods of < 1 hour, which will be complete up to periods of < 15 min (e.g. [Nelemans et al. 2001](#); [Ruiter et al. 2009](#); [Nissanke et al. 2012](#); [Lamberts et al. 2019](#); [Breivik et al. 2020](#); [Li et al. 2020](#); [Korol et al. 2022](#)). A significant number of $\mathcal{O}(10^2)$ of stellar remnant binaries – primarily those composed of two white dwarfs – discovered by *LISA* will be possible to study in combination with EM surveys (e.g. [Nelemans et al. 2004](#); [Marsh 2011](#); [Korol et al. 2017](#); [Breivik et al. 2018](#); [Tauris 2018](#); [Li et al. 2020](#)).

In the context of the *LISA* mission, stellar remnant binaries known from EM observations are often termed ‘verification binaries’, based on the idea that one can model their GW signal using EM measurements of binary’s parameters and to employ these to test *LISA* data quality (e.g. [Str er & Vecchio 2006](#); [Littenberg 2018](#); [Savalle et al. 2022](#)). In our previous work, we reviewed a sample of candidate *LISA* verification binaries following the second *Gaia* data release (DR2). This allowed us to determine distances – previously highly uncertain for most binaries – based on *Gaia*’s parallax measurements ([Kupfer et al. 2018](#); [Ramsay et al. 2018](#)). In turn, new distance estimates enabled us to evaluate the uncertainty on the expected GW signal’s amplitude and to assess the detectability of these candidate verification binaries with *LISA*. In this work we update the sample of candidates *LISA* verification binaries in a number of ways. Firstly, we include several newly discovered systems since *Gaia* DR2 (Section 2). Secondly, we re-evaluate the distances based on improved astrometry from the third *Gaia* DR3, while also taking into account their proper motion information (Section 3.3). In addition, we evaluate their detectability as well as the binary parameter estimation in a fully-Bayesian way using the up-to-date *LISA* sensitivity requirements (Section 3.4).

So far verification binaries have been (arbitrarily) defined as such based on an assumed signal-to-noise ratio (SNR) detection threshold reached at a set observation time. However, this definition relies on a few caveats. Firstly, the SNR threshold and the integration time needed to make an unambiguous identification of a (known) source is not just a matter of source’s intrinsic amplitude, but is also heavily dependent on the realization of the rest of the Galactic population (i.e. unresolved Galactic confusion foreground) that the source is competing against (e.g. figure 4 of [Korol et al. 2023](#)). In addition, the Galactic confusion foreground is dynamic: it will decrease with time as more and more sources will become detectable and will become individually resolved. Moreover, *LISA*’s orbit around the Sun will introduce a modulation in the Galactic foreground reaching its maximum when *LISA* is optimally oriented towards the Galactic center, which is where the density of Galactic sources peaks (e.g. [Petiteau 2008](#)). A prototype global fit data analysis pipeline for *LISA* demonstrated that the Galactic foreground subtraction steadily improves with time with a few $\mathcal{O}(10^3)$ binaries being identified (and subtracted) already after 1 month ([Littenberg & Cornish 2023](#)). Moreover, known binaries will be the most crucial in the early weeks/months of the mission operation in helping to validate the early performance of the instrument in comparison to pre-launch expectations. It is therefore reasonable to expect that the first data validation may be required after only a few months from the beginning of science operations. We anticipate that an integration time as short as 1-3 months would allow for basic consistency tests on the recovered parameters on a few epochs of commissioning data for several verification binaries. Given all the above, in this study we opt to call as *verification binary* a system that becomes detectable, which is judged based on the shape of the recovered posteriors on binary’s parameters rather than a SNR threshold, within 3 months of observation time with

¹ <https://sci.esa.int/web/lisa/-/61367-mission-summary>

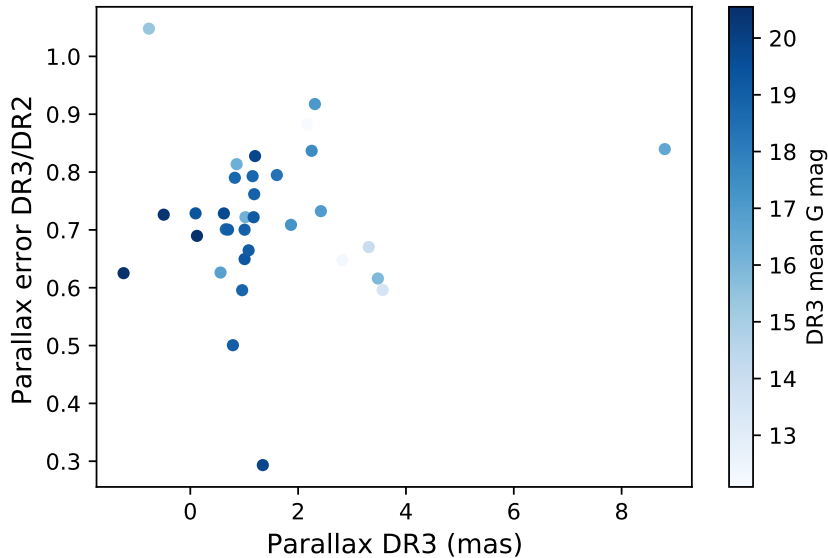


Figure 1. The error of the parallax in DR3 compared to DR2 for the verification sources in Tables 1 and 2. The color indicates the mean G mag of the source.

LISA, and we call a as *detectable binary* when it is detected after 48 months (at present set as the nominal lifetime of the mission).

2. THE SAMPLE OF COMPACT *LISA* SOURCES SINCE *Gaia* DR2

At present the catalog of candidate verification binaries includes detached (Brown et al. 2016a) and semi-detached double white dwarfs (the latter called AMCVn type binaries; see Solheim (2010) for a recent review), hot subdwarf stars with a white dwarf companion (see Geier et al. (2013); Kupfer et al. (2022); Pelisoli et al. (2021) for recent discoveries), semi-detached white dwarf-neutron star binaries (so-called ultracompact X-ray binaries; Nelemans & Jonker 2010), double neutron stars (Lyne et al. 2004) and Cataclysmic Variables (CVs, Scaringi et al. 2023). In Kupfer et al. (2018) we analyzed ~ 50 known candidates using distances derived from parallaxes provided in the *Gaia* DR2 catalog (DR2, Gaia Collaboration et al. 2018). We found that 13 candidates exceed a SNR threshold of 5 for a *LISA* mission duration of 4 years.

The Zwicky Transient Facility (ZTF) performed a dedicated high-cadence survey to find short period binaries (Kupfer et al. 2021). More than 20 new binary systems with orbital periods ranging from 7 min to ≈ 1 h have been discovered by ZTF since the beginning of science operations in March 2018 (Bellm 2014; Burdge et al. 2019a, 2020a,b; Kupfer et al. 2020a,b; van Roestel et al. 2022; Burdge et al. 2023). This new sample includes eight eclipsing systems, seven AMCVn systems, and six systems exhibiting primarily ellipsoidal variations in their light curves. Remarkably, one of the first ZTF discoveries was the shortest orbital period detached eclipsing binary system known to date, ZTF J1539+5027, with an period of just 6.91 min (Burdge et al. 2019a). Owing both to its inherently high GW frequency and large GW amplitude, ZTF J1539+5027 is expected to be one of the loudest Galactic GW sources and could reach the SNR detection threshold of ≈ 7 within a week. Littenberg & Cornish (2019) showed that for high frequency systems like ZTF J1539+5027, GW measurements will independently provide comparable levels of precision to the current EM measurement of the orbital evolution of the system, and will improve the precision to which the distance and orientation is known.

The Extremely Low Mass (ELM) White Dwarf Survey has successfully completed its observations across the footprint of the Sloan Digital Sky Survey (SDSS), and expanded their search to the Southern hemisphere (Brown et al. 2022; Kosakowski et al. 2020, 2023a). Over the last few years the ELM survey discovered several sub-hour orbital-period double degenerates, including the first double helium-core white dwarf binary (e.g. Brown et al. 2020; Kilic et al. 2021; Kosakowski et al. 2021, 2023b). It is expected that double helium-core white dwarfs and carbon/oxygen + helium-core white dwarfs dominate the population in the *LISA* band despite that they make up only 10% of the global double white dwarf population (Lamberts et al. 2019).

Moreover, several additional candidates have been found in other large-scale surveys. SDSS J1337 was discovered as a double degenerate in early SDSS-V data with an orbital period of 99 min. The spectrum shows spectral lines from both components making it a double lined system which provides precise system parameters (Chandra et al. 2021). Pelisoli et al. (2021) discovered a compact hot subdwarf binary with a massive white dwarf companion in a 99 min period orbit in the TESS sky survey. The total mass of the system is above the Chandrasekhar mass making the system a double degenerate supernova Ia progenitor. Scaringi et al. (2023) showed that three known CVs, namely WZ Sge, VW Hyi and EX Hyi, could be individually resolved after four years of *LISA* operation.

Since the release of *Gaia* DR2 a few years ago, numerous sky surveys have collectively tripled the number of identified candidate compact binaries. It’s noteworthy, however, that these surveys employ a variety of detection techniques and analysis methods, leading to heterogeneity in the presentation of results. Table 1 offers an overview of the observational results for known sources detectable by *LISA*, as reported in the respective studies. The properties of all sources compiled for this publication are accessible to the public via the *LISA* Consortium’s GitLab repository at <https://gitlab.in2p3.fr/LISA/lisa-verification-binaries>.

3. METHODS

3.1. Improvements from *Gaia* DR2 to *Gaia* DR3

In 2018 *Gaia* DR2 released full astrometric solutions, including parallaxes, and proper motions for 1.3 billion sources (Gaia Collaboration et al. 2016, 2018). The release was based on observations taken between July 2014 and May 2016. The parallaxes allowed us for the first time to calculate distances for a large sample of *LISA* detectable compact binaries. The distances in combination with the chirp mass provided the opportunity to calculate GW amplitudes and estimate the detectability for *LISA* (Kupfer et al. 2018). Until *Gaia* DR2 only a small sample of AM CVn binaries had parallax measurements using the Hubble Space telescope (Roelofs et al. 2007).

About two years after the second data release, the *Gaia* early data release (eDR3) provided full astrometric solutions for 1.4 billion sources based on 34 month of observations (Gaia Collaboration et al. 2020). The released data included one additional year of *Gaia* data leading to a higher precision in the parallaxes and proper motions compared to DR2 as well as first time parallax measurements for several *LISA* sources, including ZTFJ1905, ZTFJ0127, SDSSJ0935, V803 Cen and CR Boo. Generally, we find that the parallaxes improved by about 20% - 30% between DR2 and eDR3, in particular for faint sources (Fig. 1). Our list also contains six binaries with either a negative parallax or a parallax error close to 100%. These are ZTF J1539, ZTF J2243, V407 Vul, ZTF J1905, 4U 1830-30, and ZTF J2029. We anticipate that for these objects the distance estimate is dominated by the derived scale length prior (cf. Section 3.3). We note that distances can also be estimated through indirect methods. In particular spectroscopic distances have been used for double white dwarfs. For this work we only include parallaxes to derive distances to be independent from spectroscopic models.

In June 2022 *Gaia* data release 3 (DR3) was released. *Gaia* DR3 included the same data as eDR3 and as such astrometric solutions did not improve between eDR3 and DR3. However, DR3 included a large amount of additional information, including orbital astrometric solutions for wide binaries with a clean solution (Gaia Collaboration et al. 2022). For the remainder of the paper we will always refer to DR3 knowing that parallaxes and proper motions are the same for eDR3 and DR3.

3.2. Systems with uncertain parallax or alternative distance estimates

Here, we take the opportunity to discuss a few systems with uncertain parallax or alternative distance estimates: HM Cnc, 4U 1830–30, V407 Vul, and ZTF J1905.

HM Cnc is the only remaining system with no parallax measurement. Therefore, the distance estimate of HM Cnc remains debated. Roelofs et al. (2010) estimated a distance of 5 kpc based on its properties whereas Reinsch et al. (2007) estimated a distance of ≈ 2 kpc based on the observed flux. Most recently Munday et al. (2023) presented the discovery of $\dot{f} = (-5.38 \pm 2.10) \times 10^{-27} \text{ Hz s}^{-2}$ in HM Cnc. They concluded that HM Cnc is close to the period minimum and theoretical MESA² calculations find a mass of $\approx 1 M_{\odot}$ for the accretor and $\approx 0.17 M_{\odot}$ for the donor. This result is in strong contradiction to the results presented in Roelofs et al. (2010) based on a spectroscopic analysis. Munday et al. (2023) also discussed different ways to measure the distance to HM Cnc and found values between 2 kpc

² MESA (Modules for Experiments in Stellar Astrophysics) is an open-source 1D stellar evolution code: <https://docs.mesastar.org/en/release-r23.05.1/>

Table 1. Physical properties of the known verification and detectable binaries. Masses and inclination angles in brackets are assumed and based on evolutionary stage and mass ratio estimations. Absolute magnitudes are calculated from the *Gaia* *G*-band magnitude in combination with our distance estimate.

Source	Type	Orbital period (s)	l_{Gal} (deg)	b_{Gal} (deg)	BP-RP (mag)	M_G (mag)	m_1 (M_{\odot})	m_2 (M_{\odot})	i (deg)
Verification binaries									
HM Cnc ^{1,2}	AMCVn	321.529129(10)	206.9246	23.3952	0.246	6.54	0.55	0.27	≈ 38
ZTFJ1539 ³	DWD*	414.7915404(29)	80.7746	50.5819	-0.263	8.44	$0.61^{+0.017}_{-0.022}$	0.21 ± 0.015	$84.15^{+0.64}_{-0.57}$
ZTFJ2243 ⁴	DWD*	527.934890(32)	104.1514	-5.4496	-0.160	9.33	$0.349^{+0.093}_{-0.074}$	$0.384^{+0.114}_{-0.074}$	$81.88^{+1.31}_{-0.69}$
V407 Vul ⁵	AMCVn	569.396230(126)	57.7281	6.4006	1.535	7.76	[0.8±0.1]	[0.177±0.071]	[60]
ES Cet ⁶	AMCVn*	620.21125(30)	168.9684	-65.8632	-0.296	5.55	[0.8±0.1]	[0.161±0.064]	[60]
SDSSJ0651 ^{*7,8}	DWD*	765.206543(55)	186.9277	12.6886	0.029	9.37	0.247 ± 0.015	0.49 ± 0.02	$86.9^{+1.6}_{-1.0}$
ZTFJ0538 ⁹	DWD*	866.60331(16)	186.8104	-6.2213	0.025	8.80	0.45 ± 0.05	0.32 ± 0.03	$85.43^{+0.97}_{-0.09}$
SDSSJ1351 ¹⁰	AMCVn	939.0(7.2)	328.5021	53.1240	-0.122	7.80	[0.8±0.1]	[0.100±0.040]	[60]
AM CVn ^{11,12}	AMCVn	1028.7322(3)	140.2343	78.9382	-0.283	6.66	0.68 ± 0.06	0.125 ± 0.012	43±2
ZTFJ1905 ⁹	AMCVn*	1032.16441(62)	0.1945	1.0968	-0.066	11.47	[0.8±0.1]	[0.090±0.035]	70 ± 20
SDSSJ1908 ^{13,14}	AMCVn	1085.108(1)	70.6664	13.9349	-0.018	6.27	[0.8±0.1]	[0.085±0.034]	10 - 20
HP Lib ^{15,16}	AMCVn	1102.70(5)	352.0561	32.5467	-0.153	6.36	0.49-0.80	0.048-0.088	26-34
SDSSJ0935 ^{17,18}	DWD	1188(42)	176.0796	47.3776	0.455	9.82	0.312 ± 0.019	0.75 ± 0.24	[60]
J0526+5934 ¹⁹	DWD	1230.37467(7)	151.9201	13.2614	0.186	7.92	$0.378^{+0.066}_{-0.060}$	$0.887^{+0.110}_{-0.098}$	$57.1^{+4.3}_{-4.1}$
J1239-2041 ²⁰	DWD	1350.432(11.232)	299.2755	42.0943	-0.072	9.00	0.291 ± 0.013	$0.68^{+0.11}_{-0.06}$	71^{+8}_{-10}
TIC378898110	AMCVn	1347.96	297.0555	1.9451	0.027	6.82	[0.8±0.1]	[0.10±0.02]	74 ± 10
CR Boo ^{16,21}	AMCVn	1471.3056(500)	340.9671	66.4884	0.066	7.74	0.67-1.10	0.044-0.088	30
SDSS0634 ²²	DWD	1591.4(28.9)	176.7322	13.3211	-0.189	8.95	$0.452^{+0.070}_{-0.062}$	$0.209^{+0.034}_{-0.021}$	37 ± 7
V803 Cen ^{16,23}	AMCVn	1596.4(1.2)	309.3671	20.7262	0.232	8.44	0.78-1.17	0.059-0.109	12 - 15
Detectable binaries									
4U1820-30 ^{24,25}	UCXB	685(4)	2.7896	-7.9144	-	3.7 ⁴⁵	[1.4]	[0.069]	[60]
ZTFJ0127 ²⁶	DWD*	822.680314(43)	128.4671	-9.5102	0.191	9.26	0.75 ± 0.06	0.19 ± 0.03	[75-90]
SDSSJ2322 ²⁷	DWD	1201.4(5.9)	85.9507	-51.2104	-0.179	9.08	0.34 ± 0.02	> 0.17	[60]
PTFJ0533 ²⁸	DWD	1233.97298(17)	201.8012	-16.2238	-0.067	8.70	$0.652^{+0.037}_{-0.040}$	0.167 ± 0.030	$72.8^{+0.8}_{-1.4}$
ZTFJ2029 ⁹	DWD*	1252.056499(41)	58.5836	-13.4655	-0.054	10.27	0.32 ± 0.04	0.30 ± 0.04	$86.64^{+0.70}_{-0.40}$
PTF1J1919 ²⁹	AMCVn*	1347.354(20)	79.5945	15.5977	0.036	9.08	[0.8±0.1]	[0.066±0.026]	[60]
TIC378898110 ³⁰	AMCVn	1347.96	297.0555	1.9451	0.027	6.82	[0.8±0.1]	[0.1±0.02]	74 ± 10
CXOGBSJ1751 ³¹	AMCVn	1374.0(6)	359.9849	-1.4108	1.623	6.01	[0.8±0.1]	[0.064±0.026]	[60]
ZTFJ0722 ⁹	DWD*	1422.548655(71)	232.9930	-1.8604	-0.157	8.23	0.38 ± 0.04	0.33 ± 0.03	89.66 ± 0.22
KL Dra ³²	AMCVn	1501.806(30)	91.0140	19.1992	0.668	9.25	0.76	0.057	[60]
PTF1J0719 ³³	AMCVn	1606.2(1.2)	168.6573	24.4945	0.425	9.30	[0.8±0.1]	[0.053±0.021]	[60]
CP Eri ^{34,35}	AMCVn	1740(84)	191.7021	-52.9098	0.218	10.5	[0.8±0.1]	[0.049±0.020]	[60]
SMSSJ0338 ²¹	DWD	1836.1(31.9)	128.8576	20.7792	-0.129	8.64	0.230 ± 0.015	$0.38^{+0.05}_{-0.03}$	69 ± 9
J2322+2103 ²⁰	DWD	1918.08(21.60)	96.5151	-37.1844	0.071	8.81	0.291 ± 0.013	0.75 ± 0.26	[60]
SDSSJ0106 ³⁶	DWD	2345.76(1.73)	191.9169	31.9952	-0.223	10.30	0.188 ± 0.011	$0.57^{+0.22}_{-0.07}$	67 ± 13
SDSSJ1630 ³⁷	DWD	2388.0(6.0)	67.0760	43.3604	-0.147	9.54	0.298 ± 0.019	0.76 ± 0.24	[60]
J1526m2711 ³⁸	DWD	2417.645(37.930)	340.4437	24.1935	-0.108	9.36	0.37 ± 0.02	> 0.40 ± 0.02	[60]
SDSSJ1235 ^{39,40}	DWD	2970.432(4.320)	284.5186	78.0320	-0.219	9.27	0.35 ± 0.01	$0.27^{+0.06}_{-0.02}$	27.0 ± 3.8
SDSSJ0923 ⁴¹	DWD	3883.68(43.20)	195.8199	44.7754	-0.236	8.62	0.275 ± 0.015	0.76 ± 0.23	[60]
CD-30° 11223 ⁴²	sdB*	4231.791855(155)	322.4875	28.9379	-0.388	4.55	0.54±0.02	0.79±0.01	82.9 ± 0.4
SDSSJ1337 ⁴³	DWD	5942.952(300)	89.0428	74.0799	0.306	11.31	0.51 ± 0.01	0.32 ± 0.01	13 ± 1
HD265435 ⁴⁴	sdB	5945.917432(280)	87.0170	1.1225	-0.425	3.76	$0.63^{+0.13}_{-0.12}$	1.01 ± 0.15	64^{+14}_{-5}

[1]Strohmayer (2005), [2]Roelofs et al. (2010), [3]Burdge et al. 2019a, [4]Burdge et al. 2020b, [5]Ramsay et al. (2002), [6]Espaillat et al. (2005), [7]Brown et al. (2011), [8]Hermes et al. (2012), [9]Burdge et al. 2020a, [10]Green et al. (2018), [11]Skillman et al. (1999), [12]Roelofs et al. (2006), [13]Fontaine et al. (2011), [14]Kupfer et al. (2015), [15]Patterson et al. (2002), [16]Roelofs et al. (2007), [17]Brown et al. (2016b), [18]Kilic et al. (2014), [19]Kosakowski et al. (2023b), [20]Brown et al. (2022), [21]Provencal et al. (1997), [22]Kilic et al. (2021), [23]Anderson et al. (2005), [24]Stella et al. (1987), [25]Chen et al. (2020), [26]Burdge et al. (2023), [27]Brown et al. (2020), [28]Burdge et al. (2019b), [29]Levitan et al. (2014), [30]Green et al. (2024), [31]Wevers et al. (2016) [32]Wood et al. (2002), [33]Levitan et al. (2011), [34]Howell et al. (1991), [35]Groot et al. (2001), [36]Kilic et al. (2011b), [37]Kilic et al. (2011a), [38]Kosakowski et al. (2023a), [39]Kilic et al. (2017), [40]Breedt et al. (2017), [41]Brown et al. (2010), [42]Geier et al. (2013), [43]Chandra et al. (2021), [44]Pelisoli et al. (2021), [45] M_V taken from van Paradijs & McClintock (1994)

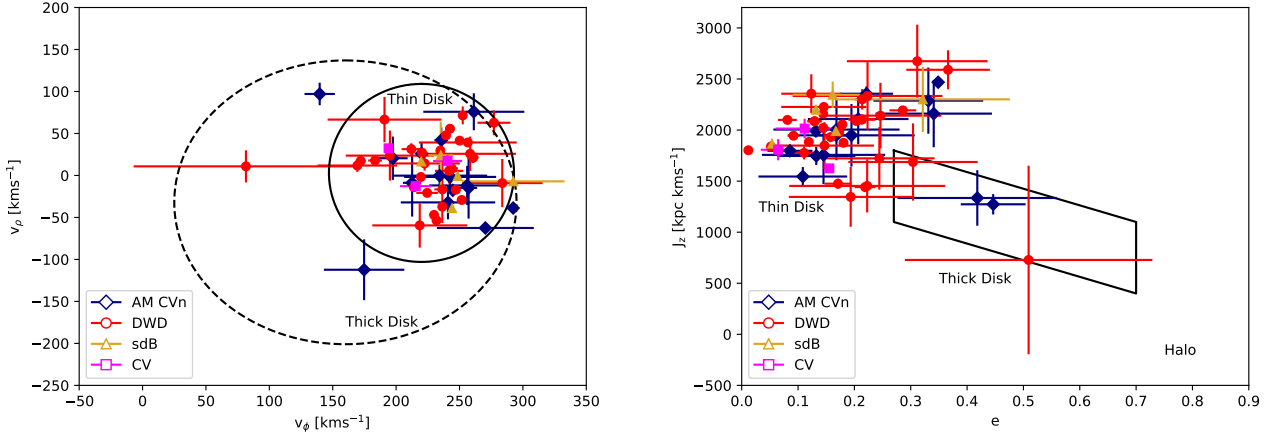


Figure 2. $V_\phi-V_\rho$ (left) and $e-J_z$ diagrams (right). The solid and dotted ellipses render the 3σ thin and thick disk contours in the $V_\phi-V_\rho$ diagram, while the solid box in the $e-J_z$ marks the thick disk region as specified by [Pauli et al. \(2006\)](#)

and 11 kpc. This shows the very large uncertainties of the system properties from EM studies. As a consequence, the expected GW amplitude also remains uncertain.

In practice, 4U 1830–30 also lacks a parallax measurement. However, it is located in the globular cluster NGC 6624, which allows for an independent distance estimate using color-magnitude diagrams with theoretical isochrones, or by using variable stars that follow known relations between their periods and absolute luminosities like RR Lyrae stars. NGC 6624 has a well-measured distance of 7972 ± 277 pc ([Baumgardt & Vasiliev 2021](#)), which we take as the distance for 4U 1830–30.

V407 Vul’s optical counterpart is dominated by a component that matches a G-type star with a blue variable ([Steehgs et al. 2006](#)). It is still unknown whether this is a chance alignment or whether V407 Vul is a triple system where an ultracompact inner binary is orbited by a G-star companion. Companions in orbits with a multi-year orbital period can present themselves in *Gaia* DR3 data, either they are listed in the non-single star tables of *Gaia* DR3 (`nss_two_body_orbit`) or they have a non-zero value in the `astrometric_excess_noise` keyword in the `gaia_source` table. The latter is non-zero if the astrometric solution shows additional perturbations to a single-source solution which could be an indication of an astrometric wobble if the G-star in V407 Vul is in a wide orbit (e.g. [Belokurov et al. 2020](#); [Penoyre et al. 2020](#)). V407 Vul is not listed in the non-single star tables of *Gaia* DR3 (`nss_two_body_orbit`) and has an `astrometric_excess_noise`=0 and `astrometric_excess_noise_sig`=0 and therefore there is no indication in the current *Gaia* DR3 data set that the G-star is a wide companion to the inner ultracompact binary. However, we note that *Gaia* DR3 is only sensitive to few years periods. Longer periods would not yet show up as astrometric wobble and therefore we cannot exclude that the G-star has a period of more than a few years.

ZTF J1905 presents a particular challenge with its uncertain *Gaia* DR3 parallax ($\varpi = 1.8652 \pm 1.5428$). This parallax value would imply the system’s absolute magnitude of ≈ 11 mag, which seems contradictory when compared to AM CVn binaries with similar orbital periods such as AM CVn or SDSS J1908. Typically, AM CVn systems in the orbital period range between 15 min - 20 min are much brighter, characterized by absolute magnitudes around 6.5 mag. There is no indication in the *Gaia* DR3 quality keywords that the parallax is problematic. Additionally, there is only modest extinction towards the direction of ZTF J1905. [Green et al. \(2019\)](#) reports $E(g-r) = 0.18$ which results in an extinction of ≈ 0.5 mag in the *Gaia*–*G* band, which is not sufficient to explain the apparent discrepancy. The distance of ZTF J1905 thus needs further investigation.

3.3. Distance estimation

Gaia DR3 provides parallaxes which can be used to determine distances. To estimate distances from the measured parallaxes we use a probability-based inference approach (e.g. [Bailer-Jones 2015](#); [Igoshev et al. 2016](#); [Astraatmadja & Bailer-Jones 2016](#); [Bailer-Jones et al. 2018](#); [Luri et al. 2018](#); [Bailer-Jones et al. 2021](#)). We follow a similar approach as described in detail in Sec. 3.2 in [Kupfer et al. \(2018\)](#). The measured parallax follows a probability distribution

and with a prior on the true distance distribution for the observed sources we can constrain the distance even if the parallax has large uncertainties. If the parallax uncertainty is below 10% - 20% the distance estimate is independent of the prior. At larger uncertainties on the distance, the distance estimate becomes more and more dependent on the prior. We apply Bayes' theorem to measure the probability density for the distance:

$$P(r|\varpi, \sigma_\varpi) = \frac{1}{Z} P(\varpi|d, \sigma_\varpi) P(d), \quad (1)$$

where d is the distance, $P(\varpi|r, \sigma_\varpi)$ is the likelihood function, that can be assumed Gaussian (Lindgren et al. 2018). $P(r)$ is the prior and Z is a normalization constant. As in Kupfer et al. (2018) we adopt an exponentially decreasing volume density prior $P(d)$

$$P(d) = \begin{cases} \frac{d^2}{2L^3} \exp(-d/L) & \text{if } d > 0 \\ 0 & \text{otherwise,} \end{cases} \quad (2)$$

where $L > 0$ is the scale length. Compared to our previous study, here we assume two values for L based on the binary's membership to the thin or thick disc as detailed below. We also stress that for systems with poor parallax measurement, the distance estimate largely depends on our assumption for L .

To estimate if our candidate *LISA* binaries are members of the thin or thick disc, for each binary we calculate Galactic kinematics, i.e. velocity components and Galactic orbit. To do this, sky position, proper motions, systemic velocities, and distances are needed. We extract proper motions from *Gaia* DR3 and calculate the distance using Eqs. (1) and (2) by setting $L = 400$ pc or $L = 795$ pc; these are typical values for L for thin disc and thick disc objects respectively³. Additionally, we use published systemic velocities, typically from radial velocity measurements. For systems with unknown systemic velocities, we assume $1 \text{ km s}^{-1} \pm 50 \text{ km s}^{-1}$. As for the distance estimate, we calculate Galactic kinematics assuming L values of 400 pc (thin discs) and 795 pc (thick disc). Using the Galactic potential of Allen & Santillan (1991) as revised by Irrgang et al. (2013), we calculate velocity in the direction of the Galactic center (V_ρ) and the Galactic rotation direction (V_ϕ), the Galactic orbital eccentricity (e), and the angular momentum in the Galactic z direction (J_z). The Galactic radial velocity V_ρ is negative towards the Galactic center, while stars that are revolving on retrograde orbits around the Galactic center have negative V_ϕ . Stars on retrograde orbits have positive J_z . Thin disk stars generally have very low eccentricities e . Population membership can be derived from the position in the $V_\rho - V_\phi$ diagram and the $J_z - e$ diagram (Pauli et al. 2003, 2006). We find that for all objects the population membership is independent of the assumption for L and we apply the appropriate value for L for the distance estimation. Fig. 2 shows the population memberships for our candidate *LISA* sources. Most systems can be identified as thin disc objects. Table 2 presents the calculated distances with the assigned value for L .

3.4. Gravitational wave parameter estimation

Gravitational radiation for a typical stellar remnant binary at mHz frequencies can be modeled as a quasi-monochromatic signal characterized by 8 parameters: GW frequency f , heliocentric amplitude \mathcal{A} , frequency derivative \dot{f} , sky coordinates (λ, β) , inclination angle ι , polarization angle ψ , and initial phase ϕ_0 . The GW frequency and amplitude are given by

$$f = 2/P_{\text{orb}}, \quad (3)$$

with P_{orb} being the binary's orbital period, and

$$\mathcal{A} = \frac{2(G\mathcal{M})^{5/3}}{c^4 d} (\pi f)^{2/3}. \quad (4)$$

This is set by the binary's distance d and chirp mass

$$\mathcal{M} = \frac{(m_1 m_2)^{3/5}}{(m_1 + m_2)^{1/5}}, \quad (5)$$

³ taken from the *Gaia* early data release 3 documentation https://gea.esac.esa.int/archive/documentation/GEDR3/Data_processing/chap_simulated/sec_cu2UM/ssec_cu2starsgal.html

Table 2. Measured EM properties (parallax, distance) and derived GW parameters of the verification binaries and detectable binaries. The distance for HM Cnc is assumed. The fractional error for the amplitude (σ_A/A) and the precision the inclination ($\Delta\iota$) is calculated for four years integration with *LISA*.

Source	f (mHz)	ϖ DR3 ^a (mas)	ϖ DR2 ^a (mas)	L (pc)	d (pc)	σ_A/A (%)	$\Delta\iota$ (deg)
Verification binaries							
HM Cnc	6.220	-	-		[5000 – 10,000]	9.5	21
ZTFJ1539	4.822	-0.4926 ± 0.5726	-0.1125 ± 0.7884	795	2469 ± 1253	1.1	0.6
ZTFJ2243	3.788	-1.2372 ± 0.6578	-1.5658 ± 1.0522	400	1756 ± 726	0.36	0.6
V407 Vul	3.512	0.0978 ± 0.2384	0.0949 ± 0.3272	400	2089 ± 684	2.0	1.9
ES Cet	3.225	0.5606 ± 0.0677	0.5961 ± 0.1081	795	1779 ± 234	2.2	2.1
SDSSJ0651	2.614	1.0071 ± 0.3091	1.0002 ± 0.4759	400	958 ± 370	1.8	0.9
ZTFJ0538	2.308	0.9617 ± 0.2866	1.1477 ± 0.4811	400	999 ± 366	2.8	1.5
SDSSJ1351	2.130	0.6584 ± 0.2197	0.5957 ± 0.3134	795	1530 ± 755	27.9	33
AM CVn	1.944	3.3106 ± 0.0303	3.3512 ± 0.0452	795	302 ± 3	12.5	23
ZTFJ1905	1.938	1.8652 ± 1.5428	-	400	697 ± 605	11.6	35
SDSSJ1908	1.843	1.0232 ± 0.0335	0.9542 ± 0.0464	400	977 ± 32	19.5	30
HP Lib	1.814	3.5674 ± 0.0313	3.6225 ± 0.0525	400	280 ± 3	13.3	24
SDSSJ0935	1.683	2.7034 ± 0.6648	-	400	395 ± 203	3.3	3.1
J0526+5934	1.625	1.1826 ± 0.0910	1.1294 ± 0.1097	400	845 ± 68	18.0	9.6
J1239-2041	1.481	1.0068 ± 0.2309	1.4054 ± 0.3297	400	972 ± 272	13.3	9.5
TIC378898110	1.483	3.2328 ± 0.0195	3.2186 ± 0.0307	400	309 ± 2		
CR Boo	1.359	2.8438 ± 0.0367	-	400	351 ± 5	19.8	29
SDSSJ0634	1.257	2.3111 ± 0.0835	2.3578 ± 0.091	400	433 ± 16	19.4	28
V803 Cen	1.253	3.4885 ± 0.0599	-	400	287 ± 5	16.1	27
Detectable binaries							
4U 1820–30	2.920	-0.7676 ± 0.2164	-0.8199 ± 0.2065	-	7972 ± 277^c	32.3	34
ZTFJ0127	2.431	0.4438 ± 0.4657	-	400	1283 ± 603	7.2	2.4
SDSSJ2322	1.665	1.1558 ± 0.2244	1.2869 ± 0.2830	400	859 ± 206	29.6	36
PTFJ0533	1.621	0.7902 ± 0.2396	0.4741 ± 0.4786	400	1173 ± 390	33.3	30
ZTFJ2029	1.597	0.1240 ± 0.9893	-1.4269 ± 1.4345	400	1095 ± 644	18.4	10
PTF1J1919	1.484	0.6229 ± 0.2385	0.5499 ± 0.3274	400	1364 ± 471	65.2	46
TIC378898110	1.484	3.2328 ± 0.0195	3.2186 ± 0.0307	400	309 ± 2	19.0	6.5
CXOGBSJ1751	1.456	0.8591 ± 0.1733	0.4994 ± 0.2130	400	1128 ± 258	48.4	41
ZTFJ0722	1.406	0.6996 ± 0.2457	0.4132 ± 0.3508	795	1461 ± 785	46.3	23
KL Dra	1.332	1.0817 ± 0.0989	1.0354 ± 0.1488	795	930 ± 91	65.4	49
PTF1J0719	1.245	1.1851 ± 0.2292	1.1436 ± 0.3009	400	840 ± 201	68.0	48
CP Eri	1.149	1.3451 ± 0.2759	0.6836 ± 0.9407	400	747 ± 203	82.6	55
SMSSJ0338	1.089	1.8675 ± 0.0562	1.8994 ± 0.0793	400	536 ± 16	43.2	40
J2322+2103	1.043	0.8261 ± 0.2503	0.6943 ± 0.3168	400	1134 ± 386	38.1	38
SDSSJ0106	0.853	1.2011 ± 0.4739	1.3521 ± 0.5726	400	824 ± 441	76.7	51
SDSSJ1630	0.837	1.1748 ± 0.1952	0.9366 ± 0.2704	400	848 ± 167	40.1	39
J1526m2711	0.827	1.6053 ± 0.1751	1.5683 ± 0.2203	400	625 ± 75	39.8	38
SDSSJ1235	0.673	2.2504 ± 0.1389	2.3319 ± 0.1660	400	446 ± 28	39.8	38
SDSSJ0923	0.515	3.4795 ± 0.0648	3.3397 ± 0.1052	400	288 ± 5	41.3	38
CD–30°11223	0.473	2.8198 ± 0.0516	2.9629 ± 0.0797	400	355 ± 7	67.8	46
SDSSJ1337	0.337	8.8007 ± 0.0440	8.6993 ± 0.0524	400	114 ± 1	32.1	35
HD265435	0.336	2.1666 ± 0.0554	2.1994 ± 0.0628	400	461 ± 12	70.6	54

^aGaia Collaboration et al. (2018), ^bGaia Collaboration et al. (2020), ^cBaumgardt & Vasiliev (2021)

for component masses m_1 and m_2 . The frequency derivative \dot{f} is expected to follow the gravitational radiation equation:

$$\dot{f} = \frac{96}{5} \frac{(GM)^{5/3}}{\pi c^5} (\pi f)^{11/3}. \quad (6)$$

To forecast *LISA* observations of the known binaries we use the VBMC sampler in LDASOFT (Littenberg et al. 2020). The sampler uses a parallel tempered Markov Chain Monte Carlo algorithm with delta-function priors on the orbital period and sky location of the binary based on the EM observations (cf. Table 1). The priors on the remaining parameters are uniform in log amplitude and cosine inclination with the start value for the inclination being set to the measured values for systems with constraints on the inclination and set to 60 deg for unconstrained systems. The sampler is also marginalizing over the first time derivative of the frequency, polarization angle, and initial phase of the binary, all of which are considered nuisance parameters for this study. Because this is a targeted analysis of known binaries the trans-dimensional sampling capabilities in LDASOFT are disabled and the algorithm uses a single template to recover the signal – effectively a delta function prior on the model. In this configuration, results for binaries below the detection threshold are used to set upper limits on the GW amplitude parameter.

The data being analyzed are simulated internally by VBMC and include stationary Gaussian noise with the same instrument noise spectrum as was used for the *LISA* Data Challenges (LDCs) in Challenge 2a⁴ plus an estimated astrophysical foreground from the unresolved Galactic binaries as described in Cornish & Robson (2017). The analysis ignores any correlations, contamination, or additional statistical uncertainty caused by the presence of other signals in the data, and also treats the astrophysical foreground as a stationary noise source. Relaxing these simplifying assumptions will be most relevant for binaries where the astrophysical foreground dominates the instrument noise spectrum at GW frequencies $\lesssim 3$ mHz but is currently beyond the scope of this analysis (considering overlap with other sources) or capabilities of the sampling algorithm (considering non-stationary noise).

4. RESULTS

We analyze 55 verification binary candidates in total using the VBMC sampler in LDASOFT for increasingly longer *LISA* mission science operation time: 1, 3, 6, 12, 36 and 48 months. We remind the reader that we perform a “targeted” analysis by fixing – using delta-function priors – binary’s sky position and orbital period to the values provided by EM measurements; additionally, we marginalize over \dot{f} , ψ and ϕ_0 (cf. Section 3.4). Differently from our previous work to assess the detectability of a binary, instead of evaluating the SNR we look at the binary’s GW parameters posterior samples. We consider the binary as *detectable* if the GW amplitude parameter is constrained away from the minimum value allowed by the prior. This is most readily identifiable by looking at the two dimensional posterior distribution in the GW amplitude-inclination plane, where a detectable binary will have closed contours in the posterior. We call as *verification binary* a system that becomes detectable (as explained in Sec. 1) within 3 months of observation time with *LISA* and we call as *detectable binary* when it is detected after 48 months of observation time with *LISA*. We introduce this distinction to highlight the use of verification binaries for the early data validations, e.g. in preparation for the first data release.

Our results show that an integration time as short as 1-3 months would allow for basic consistency tests on the recovered parameters on a few epochs of commissioning data for 9-18 verification binaries; while extending our definition up to 6 month increases the sample by only four additional binaries. To clarify the difference between a verification, detectable and non-detectable binary, in Fig. 3 we show posteriors of the binary’s inclination and GW amplitude for three examples: ZTFJ1539 (~ 7 min orbital period, verification binary), ZTFJ2029 (~ 21 min, detectable binary) and SDSSJ0822 (~ 40 min, non-detectable binary). ZTFJ1539 shows closed contours already after 1 month of observations, which become increasingly narrow as observation time increases. Being detectable so early on, it is highly likely that ZTFJ1539 can be used as one of *LISA*’s verification binary. ZTFJ2029 represents an intermediate case as initially its posterior contours are open at low amplitude, but they close after 36 months at which point we classify this binary as detectable. Finally, we show the case of SDSSJ0822 which, based on the same reasoning as above, we classify as non detectable. Right panels of Fig. 3 illustrate how *LISA*’s fractional error on GW amplitude \mathcal{A} and inclination ι (orange lines) improve over time. Assuming that EM measurement would not improve in the future, which is plausible if no additional EM measurements are taken between now and when *LISA* will fly, we show the estimate of the same parameters based on the current EM measurement (gray lines) for comparison.

⁴ <https://lisa-ldc.lal.in2p3.fr/challenge2a>

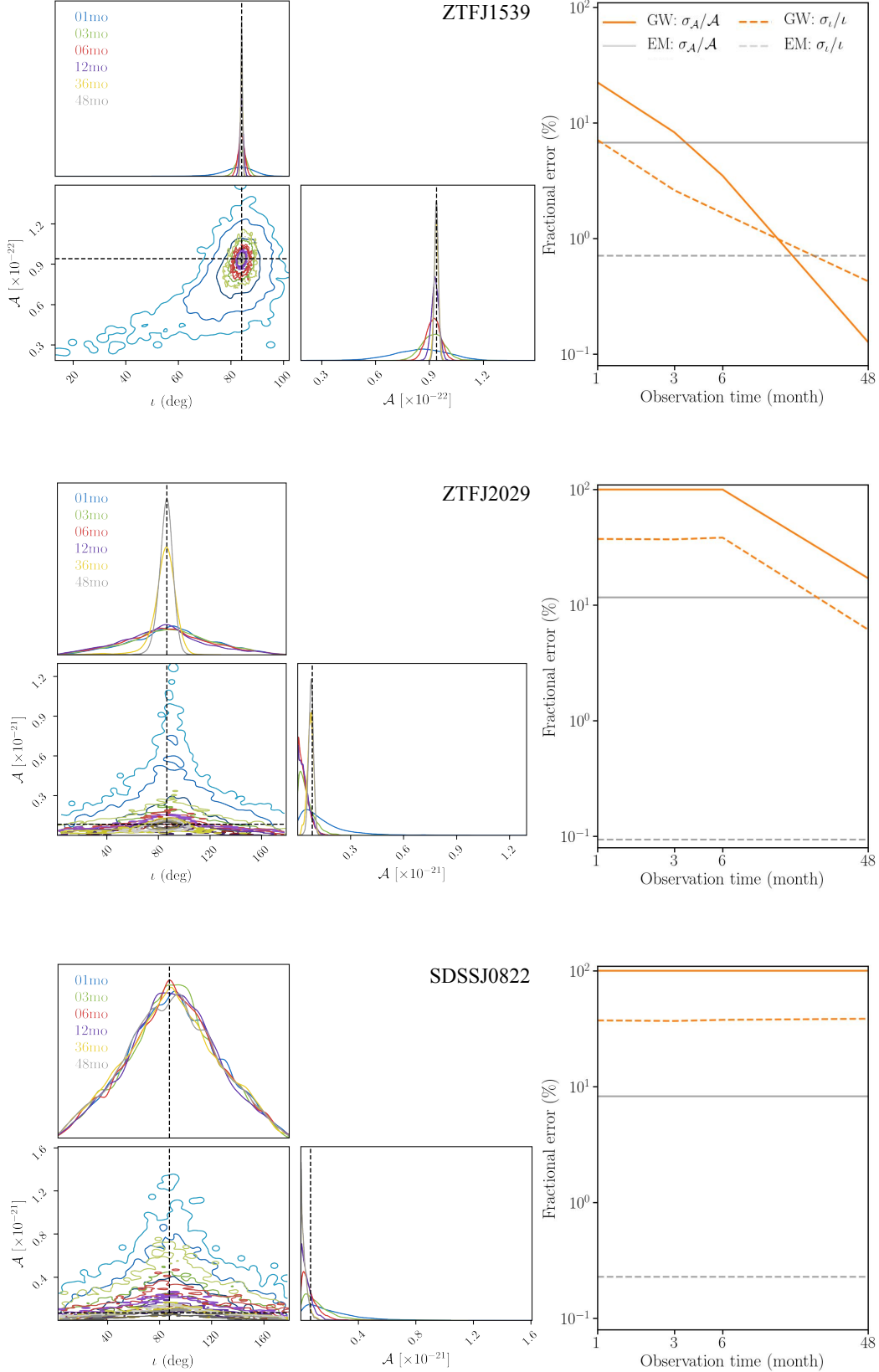


Figure 3. Three examples of posteriors for binary’s inclination and GW amplitude; from top to bottom these are: ZTFJ1539 (verification binary), ZTFJ2029 (detectable binary) and SDSSJ0822 (non-detectable binary). On the left we show how the estimated fractional error on the amplitude σ_A/A and inclination σ_i/i change as the functions of observation time; for comparison we also show current EM constrains and assuming that these won’t change before *LISA*’s launch (cf. Table 1 and 2).

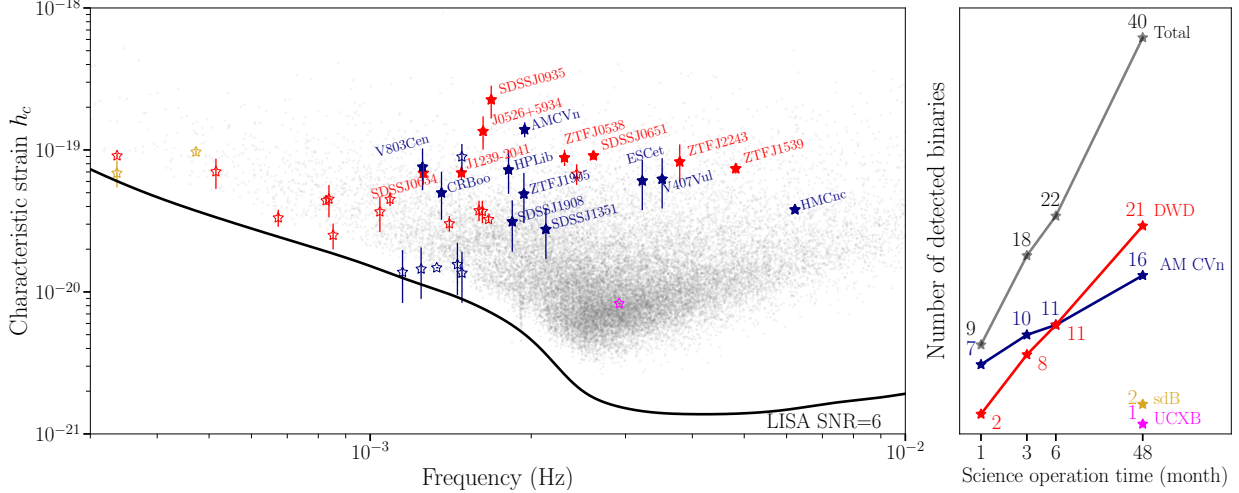


Figure 4. *Left panel:* Characteristic strain - frequency plot for detectable and verification binaries: AM CVns in blue, DWDs in red, sdBs in yellow and UCXB in magenta. Filled stars represent binaries detectable within 3 month of observations, which we call here ‘verification binaries’. The error bars on characteristic strain show 1σ uncertainty evaluated by generating random samples from EM measurement uncertainties on binary component masses and distances presented in Table 1 and 2. Black solid line represents *LISA*’s sensitivity curve that accounts for the instrumental noise (*LISA Science Study Team 2018*) and Galactic confusion foreground (*Babak et al. 2017*). For comparison in gray we show a mock Galactic DWD population detectable with *LISA* from *Wilhelm et al. (2021)*. *Right panel:* Number of detected binaries as a function of science operation time.

Based on our definition above, overall we find 40 binaries detectable with *LISA* within 4 yr of science operations, out of which we classify 18 (10 AM CVns + 8 DWDs) as verification binaries, i.e. detectable within the first 3 months. We list their properties in Table 1 and 2. The summary of our results is presented in Fig. 4. In the left panel we show characteristic strain - frequency plot for all detectable binaries: AM CVns in blue, DWDs in red, sdBs in yellow and UCXB in magenta. Filled stars represent *LISA* verification binaries, empty stars are detectable binaries within the nominal mission life time (48 month). We compute the error bars on characteristic strain by generating random samples from EM measurement uncertainties on binary component masses and distance (cf. Table 1 and 2); in the figure we plot 1σ uncertainty based on our random samples. For comparison we also show a mock Galactic DWD population of *Wilhelm et al. (2021)* in gray, as well as the *LISA* sensitivity curve at SNR=6 as black solid line. The comparison reveals that the current sample of known binaries is mainly representative of the ‘loudest’ GW sources in the Milky Way, while the majority is yet to be discovered in more remote parts of our Galaxy inaccessible for EM observatories (see figure 15 of *Amaro-Seoane et al. 2023*). In the right panel of Fig. 4 we show the detection statistic as a function of the science operation time with a break down for different types of binaries showing that in increased science operation for *LISA* will lead to a larger number of detected binaries in the *LISA* data. We note that in our study none of the CVs will be detectable within four years of *LISA* observations.

In our previous study *Kupfer et al. (2018)*, we identified 13 detectable binaries. The reasons for the difference are multiple. Firstly, the sample of candidate verification binaries has tripled in the past few years (cf. Section 2). Secondly, some distance estimates have improved between *Gaia* DR2 and DR3 (this is, for example, true for CXOGBSJ1751 and SDSSJ163); for some binaries (ZTFJ0127, ZTFJ1905, SDSSJ0935, V803 Cen, CR Boo) parallaxes were not available as part of the DR2. Most importantly, we also change our criterion for the detectability moving away from a SNR based definition. Recently, *Finch et al. (2023)* have used our catalog for a number of *LISA* data analysis investigations by performing a Bayesian parameter estimation with the BALROG code (*Roebber et al. 2020; Buscicchio et al. 2021; Klein et al. 2022*). They verified that binaries with SNR<6 generally display broad posteriors, with no clear peaks and with amplitude parameter being inconsistent with zero. Thus, they adopted the SNR threshold of 6 as criterion for the detectability with *LISA*. They found that up to 14 binaries can be detected within 3 months of observations (see their figures 4 and B1). This result is in agreement with ours considering new binaries that have been added to the list of candidates in our study.

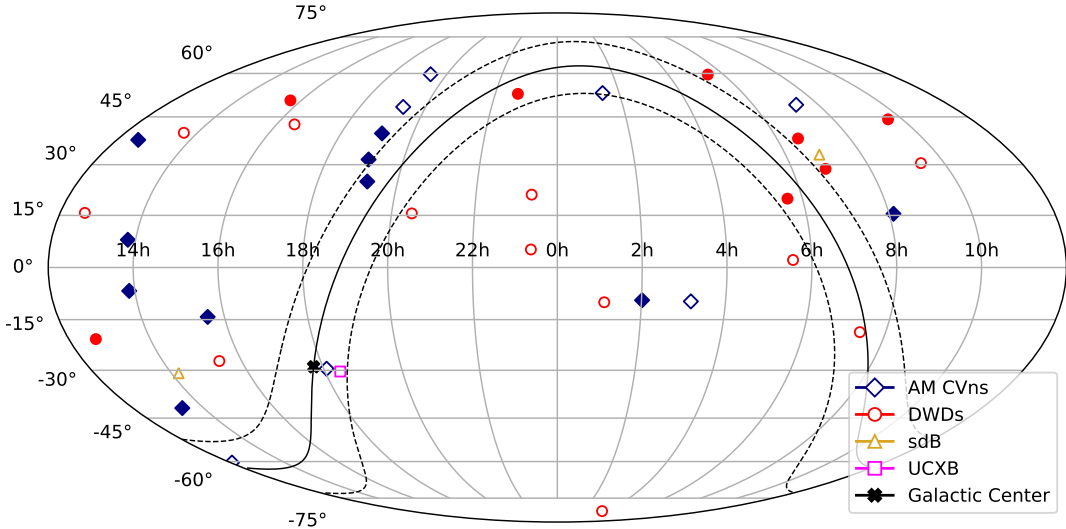


Figure 5. The position of the *LISA* binaries on the sky in an equatorial projection, with the Galactic plane ($\pm 10^\circ$) shown by the full and dashed lines. Filled symbols are verification binaries whereas open symbols are detectable binaries.

We report estimated fractional error on the GW amplitude ($\sigma_{\mathcal{A}}/\mathcal{A}$) and the estimated precision for the inclination (Δi) that can be reached after 4 years of observation in Table 2. On average, for verification binaries the amplitude is forecasted to be measured to $\sim 10\%$, while the inclination is expected to be determined with $\sim 15^\circ$ precision. For detectable binaries these average errors decrease to $\sim 50\%$ and to $\sim 40^\circ$ respectively. From the table one can deduce that the measurements depend on the binary’s frequency (generally improving with increasing frequency) and strength of the signal (with verification binaries being better characterized than detectable binaries). Our estimates are in good agreement with Finch et al. (2023, see their table 2).

Figures 5 and 6 illustrate respectively the position of detectable (empty symbols) and verification (filled symbols) binaries on the sky and on the *Gaia* Hertzsprung-Russell (HR) diagram. Both reveal different limitations of the current sample. Figure 5 shows that although the size of the candidate *LISA* binaries is progressively growing, it is still biased towards the Northern Hemisphere (where the majority of surveys have been conducted so far), and to high latitudes (to avoid the dust extinction and crowding in the Galactic plane). From observations of bright non-degenerate stars we know that the Galactic stellar population is concentrated in the disc (region in between dashed lines) peaking towards the Galactic center (thick black cross in Fig. 5), and so we expect *LISA* detectable binaries to follow the same distribution (e.g. see Szekerczes et al. 2023). Figure 6 shows our sample of *LISA* sources compared to the absolute magnitudes (M_G) and colors ($BP - RP$) of *Gaia*’s sample of stars with parallax uncertainty below 1% (gray points). The plot shows a bias towards sources brighter and bluer compared to objects on the white dwarf track where most DWDs are expected. We note that on the HR diagram we use down-pointing triangles to highlight that our absolute magnitude estimates in our sample are to be interpreted as upper limits. This is because for all candidate *LISA* binaries the extinction, which is necessary to convert apparent *G* magnitudes measured by *Gaia* magnitudes into absolute magnitudes M_G , is not well measured. Potential *LISA* sources with larger magnitudes can only be observed up to a couple kpc with current surveys, which limits the volume where *LISA* binaries can be detected. In contrast to EM searches, *LISA* measures directly the amplitude of GW waves, rather than the energy flux. Thus, the observed GW signal scales as $1/d$, rather than $1/d^2$, allowing *LISA* to detect binaries at larger distances – potentially within the entire Milky Way volume – than in the traditional EM observational bands.

5. DISCUSSION

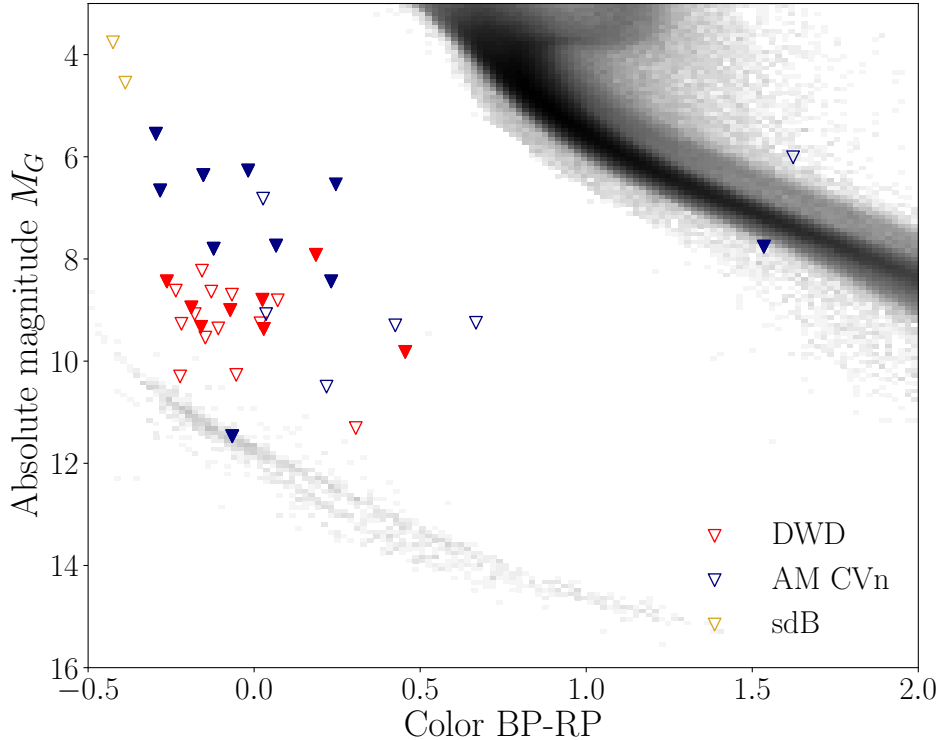


Figure 6. Verification binaries (in color) on the *Gaia* Hertzsprung-Russell diagram (in gray). Down-pointing triangles are used to symbolize that absolute magnitude estimates are to be interpreted as upper limits because we do not account for extinction. As before, filled symbols represent verification binaries whereas open symbols represent detectable binaries.

5.1. Limitations of the current sample and prospects to expand the sample

The currently known sample of candidate *LISA* verification binaries is inhomogeneous and biased. This bias is evident in the sky distribution (Fig. 5), predominantly favoring the Northern hemisphere with 60% of *LISA* sources. Furthermore, the HR diagram (Fig. 6) reveals an over-representation of sources above the main white dwarf track. This is due to the nature of magnitude-limited ground-based surveys favoring brighter sources. Finally, a significant challenge lies in the multitude of detection and analysis methods, leading to a non-uniformity in presenting parameters of these binaries. Parameters are presented in varied ways: with a $1 - \sigma$ error, no constraints, approximations or limits. To facilitate more effective future multi-messenger studies, it is essential to develop uniform analysis methods that provide a standard set of prior information.

Between *Gaia* DR2 and *Gaia* DR3 the number of detectable *LISA* sources has tripled which can be explained by the large number of sky surveys that came online over the last few years. This will improve even more over the next decade with many additional surveys coming online over the next few years. As proven in the past, photometric and spectroscopic surveys are ideal tools to find new *LISA* binaries and complement each other. Eclipses or tidal deformation lead to photometric variability on the orbital period, whereas compact *LISA* binaries show up in multi-epoch spectroscopy due to large radial velocity shifts between individual spectra.

SDSS-V is an all-sky, multi-epoch spectroscopic survey which started operations in 2020 and will provide spectra for a few million sources (Kollmeier et al. 2017). Already in early SDSS-V data Chandra et al. (2021) discovered a new detectable *LISA* binary. Other spectroscopic ongoing or upcoming spectroscopic surveys include LAMOST (Zhao et al. 2012), 4MOST (de Jong et al. 2019) or WEAVE (Dalton et al. 2014). The Asteroid Terrestrial-impact Last Alert System (ATLAS, Tonry et al. 2018; Heinze et al. 2018) and the Gravitational-wave Optical Transient Observer (GOTO, Steeghs et al. 2022) are ongoing photometric sky surveys with telescopes located in both hemispheres allowing for an all-sky coverage for both surveys. Their cadence and sky coverage are well suited to find *LISA* detectable binaries. BlackGEM is a photometric sky survey covering the Southern hemisphere which has started operations in

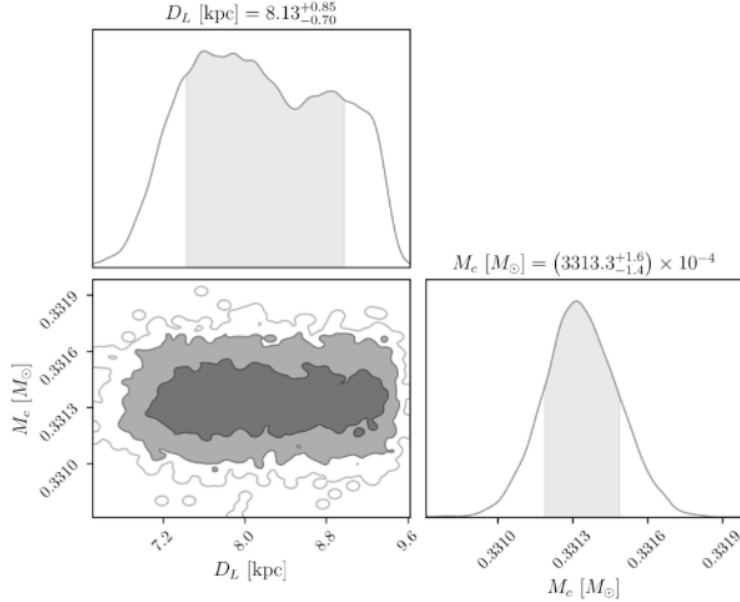


Figure 7. Posterior distribution for HM Cnc’s expected chirp mass and distance precision predicted for four years of *LISA* observations.

2023 (Bloemen et al. 2015). Part of the BlackGEM operations will be the BlackGEM Fast Synoptic Survey which is a continuous high cadence survey of individual fields in the Southern hemisphere. The cadence is ideal to discover new *LISA* detectable binaries. First light for the Vera Rubin telescope is expected in 2024. The telescope will perform the Legacy Survey of Space and Time (LSST) covering the Southern hemisphere down to 24 mag (per single exposure) going much deeper and hence covering a significantly larger volume than current sky surveys. Although the cadence is expected to be not ideal for *LISA* binaries, LSST will collect sufficient photometric observations over 10 years to be able to discover *LISA* binaries. The next large *Gaia* data release (DR4) is expected to include precision time series photometry of ≈ 70 epochs for each object taken over a five year time frame. Euclid is a space mission operating in the near-infrared and visible bands which was launched in 2023 with an unprecedented sky resolution of almost one order of magnitude better compared to ground based observatories. Part of Euclid’s operation will be the Euclid deep survey covering a total of 40 sqd for three distinct fields. Each field will get several tens of epochs over its nominal mission time of six years with a depth of ≈ 25 mag for each epoch in the near-infrared bands (Laureijs et al. 2011). Finally, in the late 2020s the Nancy Roman space telescope will conduct a wide-field survey with the same sky resolution as Euclid down to 24 mag. Therefore, we expect that the number of *LISA* detectable sources will significantly increase before the *LISA* launches providing a large sample of multi-messenger sources (e.g. Korol et al. 2017; Li et al. 2020).

5.2. Focus for future EM efforts

EM measurement of a binary’s inclination will significantly inform *LISA*’s data analysis and parameter estimation, particularly for nearly edge-on systems (Table 1). As Shah et al. (2012) outlined, EM inclination data enhances GW amplitude measurement due to the strong correlation between amplitude and inclination parameters in GW data (Fig. 3). This improves chirp mass and distance determination. Also, Finch et al. (2023) demonstrated the advantage of EM prior information in reducing detection time versus a blind search. They show that after the binary has been detected, further parameter estimation improvements are inclination-dependent; face-on sources benefit greatly from prior inclination knowledge, with amplitude measurement improvement increasing with observation time (their figure 5). This underscores the importance of binary inclination data from EM observations for future *LISA* data analysis. However, 40% of current sources lack inclination measurement. These are primarily non-eclipsing sources where measurement is non-trivial.

Determining \dot{f} from GW data alone can be challenging for low-frequency ($f < 2$ mHz) and/or low-SNR binaries. On the other hand, high-precision \dot{f} measurement is achievable via EM observations for eclipsing sources through ground-

based eclipse timing measurements over long baselines (e.g., >10 years). [Shah & Nelemans \(2014\)](#) demonstrated the accuracy improvement on the chirp mass when adding EM \dot{f} data to GW analysis.

Knowledge of distance (d) or parallax (ϖ) is also crucial for characterizing *LISA* binaries. As mentioned in Section 3.3, parallax constrains the luminosity distance, directly affecting GW amplitude (Eq. 4). *LISA*'s GW frequency and amplitude measurements, coupled with *Gaia*-based parallax, allow binary chirp mass determination (solving Eq. 4 for \mathcal{M}) without measuring \dot{f} , usually required for chirp mass determination from GW data (Eq. 6). Error propagation illustrates that chirp mass error and parallax error are linearly related ($\sigma_{\mathcal{M}}/\mathcal{M} \propto \varpi\sigma_{\varpi}$), meaning that parallax measurement improvement directly enhances chirp mass estimation. This method recovers chirp masses for binaries at *LISA*'s low-frequency end and for interacting binaries, whose \dot{f} contains an astrophysical contribution (e.g. [Breivik et al. 2018](#); [Littenberg & Cornish 2019](#)), as in verification binaries AM CVn and HP Lib.

The forthcoming *Gaia* DR4, based on 66 months of data collection, should mark significant improvement over the DR3 (34 months). An estimated improvement factor for parallax errors of ~ 0.7 can be expected (using $\sigma_{\varpi} \propto (T_{\text{DR3}}/T_{\text{DR4}})^{0.5} \sim (34/66)^{0.5}$), with T_{DR3} and T_{DR4} expressed in months, see [Gaia Collaboration et al. 2018](#). Additional enhancements in *Gaia* data quality are anticipated, given the indicative mission extension until 2025⁵, allowing for data collection up to a total of 10 years. However, very distant or faint systems might never have a reliable parallax measurement from *Gaia*. If the period is sufficiently short, *LISA* will provide an \dot{f} measurement which can break the degeneracy between chirp mass and distance and as such *LISA* will provide an independent distance measurement. Fig. 7 shows the expected distance measurement from *LISA* for HMCnc. We expect an uncertainty of about 1.5 - 2 kpc, which is significantly better than any current estimates from EM observations (cf. Section 3.2).

6. SUMMARY AND CONCLUSIONS

In this work we derive updated distances and kinematics for 55 verification binary candidates using parallaxes and proper motions from *Gaia* DR3. Using these distances and system properties we calculate the detectability for each source after 1, 3, 6 and 48 months of *LISA* observations. We find that 18 verification binaries can be detected after 3 months of *LISA* observations and used for science verification. An additional 22 sources will be detected after 48 months of *LISA* observations totaling the number of detectable *LISA* to a total of 40 sources. The sources consist of 21 DWDs, 16 AMCVn binaries, 2 hot subdwarf binaries and 1 ultracompact X-ray binary. In particular AMCVn and HPLib are verification binaries with parallax errors below 1% making them ideal validation sources.

The number of detectable *LISA* binaries has tripled over the last five years since [Kupfer et al. \(2018\)](#). That is mainly due to increasing number of large scale sky surveys, in particular the ELM survey and ZTF were driving the discoveries over the last few years. However, even with the large increase in sources, the sample is still strongly biased towards luminous binaries and sources located in the Northern hemisphere. However, we predict that the number of systems will continue to increase significantly over the next few years with additional large scale surveys coming online over the next few years and strategies need to be developed to perform efficient follow-up for each source before *LISA* launches.

For sources without a measured \dot{f} , generally the distance is required to measure the chirp mass. The error on the parallax scales linearly with the error on the chirp mass. We find that the parallax precision has improved by 20% – 30% between *Gaia* DR2 and DR3 and another $\approx 30\%$ improvement is expected for *Gaia* DR4. We find that on average for verification binaries the GW amplitude is expected to be measured to $\approx 10\%$ precision, while the inclination is expected to be determined with $\approx 15^\circ$ precision. For detectable binaries these average errors decrease to $\approx 50\%$ and to $\approx 40^\circ$ respectively. At present, 40% of the *LISA* sources have no measured inclination from EM observations. These are mainly non-eclipsing sources where it is non-trivial to measure an inclination angle and it might be that no progress will be made on the inclination before *LISA*. Therefore, even an uncertain inclination measurement from *LISA* will be extremely valuable.

Properties for all sources are collected for this publication is publicly available on the *LISA* Consortium GitLab repository <https://gitlab.in2p3.fr/LISA/lisa-verification-binaries>. We wish to keep this list up-to-date for the Consortium and more broader community. Thus we welcome submission requests for new binaries and/or other suggestions.

⁵ <https://www.cosmos.esa.int/web/gaia/release>

1 While working on this study, we were deeply saddened by the loss of Professor Tom Marsh, a world-leading expert
 2 on compact binary star systems and a visionary in recognizing the potential of the *LISA* mission for the study of these
 3 binaries. Professor Marsh's profound knowledge and pioneering insights were invaluable to this study. His enthusiasm
 4 and dedication to the field were not only inspiring but also instrumental in shaping the direction of our work.

5 TK acknowledges support from the National Science Foundation through grant AST #2107982, from NASA through
 6 grant 80NSSC22K0338 and from STScI through grant HST-GO-16659.002-A. Co-funded by the European Union (ERC,
 7 CompactBINARIES, 101078773). Views and opinions expressed are however those of the author(s) only and do not
 8 necessarily reflect those of the European Union or the European Research Council. Neither the European Union nor
 9 the granting authority can be held responsible for them. VK acknowledges support from the Netherlands Research
 10 Council NWO (Rubicon 019.183EN.015 grant). PJG is partially supported by NRF SARChI grant 111692. Armagh
 11 Observatory & Planetarium is core funded by the Northern Ireland Executive through the Dept for Communities. SS
 12 acknowledges support from the DLR grant number / Förderkennzeichen: 500Q1801.

13 This work presents results from the European Space Agency (ESA) space mission Gaia. Gaia data are being
 14 processed by the Gaia Data Processing and Analysis Consortium (DPAC). Funding for the DPAC is provided by
 15 national institutions, in particular the institutions participating in the Gaia MultiLateral Agreement (MLA). The Gaia
 16 mission website is <https://www.cosmos.esa.int/gaia>. The Gaia archive website is <https://archives.esac.esa.int/gaia>

Facilities: Gaia

Software: `Matplotlib` (Hunter 2007), `Astropy` (Astropy Collaboration et al. 2013, 2018), `Numpy` (Oliphant 2015),
 LDASOFT (Littenberg et al. 2020)

REFERENCES

- Allen, C., & Santillan, A. 1991, *RMxAA*, 22, 255
- Amaro-Seoane, P., Audley, H., Babak, S., et al. 2017, arXiv e-prints, arXiv:1702.00786.
<https://arxiv.org/abs/1702.00786>
- Amaro-Seoane, P., Andrews, J., Arca Sedda, M., et al. 2023, *Living Reviews in Relativity*, 26, 2,
 doi: [10.1007/s41114-022-00041-y](https://doi.org/10.1007/s41114-022-00041-y)
- Anderson, S. F., et al. 2005, *AJ*, 130, 2230,
 doi: [10.1086/491587](https://doi.org/10.1086/491587)
- Astraatmadja, T. L., & Bailer-Jones, C. A. L. 2016, *ApJ*, 832, 137, doi: [10.3847/0004-637X/832/2/137](https://doi.org/10.3847/0004-637X/832/2/137)
- Astropy Collaboration, Robitaille, T. P., Tollerud, E. J., et al. 2013, *A&A*, 558, A33,
 doi: [10.1051/0004-6361/201322068](https://doi.org/10.1051/0004-6361/201322068)
- Astropy Collaboration, Price-Whelan, A. M., Sipőcz, B. M., et al. 2018, *AJ*, 156, 123, doi: [10.3847/1538-3881/aabc4f](https://doi.org/10.3847/1538-3881/aabc4f)
- Babak, S., Gair, J., Sesana, A., et al. 2017, *Phys. Rev.*, D95, 103012, doi: [10.1103/PhysRevD.95.103012](https://doi.org/10.1103/PhysRevD.95.103012)
- Bailer-Jones, C. A. L. 2015, *PASP*, 127, 994,
 doi: [10.1086/683116](https://doi.org/10.1086/683116)
- Bailer-Jones, C. A. L., Rybizki, J., Fouesneau, M., Demleitner, M., & Andrae, R. 2021, *AJ*, 161, 147,
 doi: [10.3847/1538-3881/abd806](https://doi.org/10.3847/1538-3881/abd806)
- Bailer-Jones, C. A. L., Rybizki, J., Fouesneau, M., Mantelet, G., & Andrae, R. 2018, *AJ*, 156, 58,
 doi: [10.3847/1538-3881/aacb21](https://doi.org/10.3847/1538-3881/aacb21)
- Baumgardt, H., & Vasiliev, E. 2021, *MNRAS*, 505, 5957,
 doi: [10.1093/mnras/stab1474](https://doi.org/10.1093/mnras/stab1474)
- Bellm, E. 2014, in *The Third Hot-wiring the Transient Universe Workshop*, ed. P. R. Wozniak, M. J. Graham, A. A. Mahabal, & R. Seaman, 27–33.
<https://arxiv.org/abs/1410.8185>
- Belokurov, V., Penoyre, Z., Oh, S., et al. 2020, *MNRAS*, 496, 1922,
 doi: [10.1093/mnras/staa152210.48550/arXiv.2003.05467](https://doi.org/10.1093/mnras/staa152210.48550/arXiv.2003.05467)
- Bloemen, S., Groot, P., Nelemans, G., & Klein-Wolt, M. 2015, in *Astronomical Society of the Pacific Conference Series*, Vol. 496, *Living Together: Planets, Host Stars and Binaries*, ed. S. M. Rucinski, G. Torres, & M. Zejda, 254
- Breedt, E., Steeghs, D., Marsh, T. R., et al. 2017, *MNRAS*, 468, 2910, doi: [10.1093/mnras/stx430](https://doi.org/10.1093/mnras/stx430)
- Breivik, K., Kremer, K., Bueno, M., et al. 2018, *ApJL*, 854, L1, doi: [10.3847/2041-8213/aaa23](https://doi.org/10.3847/2041-8213/aaa23)
- Breivik, K., Coughlin, S., Zevin, M., et al. 2020, *ApJ*, 898, 71, doi: [10.3847/1538-4357/ab9d85](https://doi.org/10.3847/1538-4357/ab9d85)
- Brown, W. R., Gianninas, A., Kilic, M., Kenyon, S. J., & Allende Prieto, C. 2016a, *ApJ*, 818, 155,
 doi: [10.3847/0004-637X/818/2/155](https://doi.org/10.3847/0004-637X/818/2/155)
- Brown, W. R., Kilic, M., Allende Prieto, C., & Kenyon, S. J. 2010, *ApJ*, 723, 1072,
 doi: [10.1088/0004-637X/723/2/1072](https://doi.org/10.1088/0004-637X/723/2/1072)

- Brown, W. R., Kilic, M., Bédard, A., Kosakowski, A., & Bergeron, P. 2020, *ApJL*, 892, L35, doi: [10.3847/2041-8213/ab8228](https://doi.org/10.3847/2041-8213/ab8228)
- Brown, W. R., Kilic, M., Hermes, J. J., et al. 2011, *ApJL*, 737, L23, doi: [10.1088/2041-8205/737/1/L23](https://doi.org/10.1088/2041-8205/737/1/L23)
- Brown, W. R., Kilic, M., Kenyon, S. J., & Gianninas, A. 2016b, *ApJ*, 824, 46, doi: [10.3847/0004-637X/824/1/46](https://doi.org/10.3847/0004-637X/824/1/46)
- Brown, W. R., Kilic, M., Kosakowski, A., & Gianninas, A. 2022, *ApJ*, 933, 94, doi: [10.3847/1538-4357/ac72ac](https://doi.org/10.3847/1538-4357/ac72ac)
- Burdge, K. B., Coughlin, M. W., Fuller, J., et al. 2019a, *Nature*, 571, 528, doi: [10.1038/s41586-019-1403-0](https://doi.org/10.1038/s41586-019-1403-0)
- Burdge, K. B., Fuller, J., Phinney, E. S., et al. 2019b, *ApJL*, 886, L12, doi: [10.3847/2041-8213/ab53e5](https://doi.org/10.3847/2041-8213/ab53e5)
- Burdge, K. B., Prince, T. A., Fuller, J., et al. 2020a, *ApJ*, 905, 32, doi: [10.3847/1538-4357/abc261](https://doi.org/10.3847/1538-4357/abc261)
- Burdge, K. B., Coughlin, M. W., Fuller, J., et al. 2020b, *ApJL*, 905, L7, doi: [10.3847/2041-8213/abca91](https://doi.org/10.3847/2041-8213/abca91)
- Burdge, K. B., El-Badry, K., Rappaport, S., et al. 2023, *ApJL*, 953, L1, doi: [10.3847/2041-8213/ace7cf](https://doi.org/10.3847/2041-8213/ace7cf)
- Buscicchio, R., Klein, A., Roebber, E., et al. 2021, *PhRvD*, 104, 044065, doi: [10.1103/PhysRevD.104.044065](https://doi.org/10.1103/PhysRevD.104.044065)
- Chandra, V., Hwang, H.-C., Zakamska, N. L., et al. 2021, *ApJ*, 921, 160, doi: [10.3847/1538-4357/ac2145](https://doi.org/10.3847/1538-4357/ac2145)
- Chen, W.-C., Liu, D.-D., & Wang, B. 2020, *ApJL*, 900, L8, doi: [10.3847/2041-8213/abae66](https://doi.org/10.3847/2041-8213/abae66)
- Cornish, N., & Robson, T. 2017, *Journal of Physics: Conference Series*, 840, 012024, doi: [10.1088/1742-6596/840/1/012024](https://doi.org/10.1088/1742-6596/840/1/012024)
- Dalton, G., Trager, S., Abrams, D. C., et al. 2014, in *Society of Photo-Optical Instrumentation Engineers (SPIE) Conference Series*, Vol. 9147, *Ground-based and Airborne Instrumentation for Astronomy V*, ed. S. K. Ramsay, I. S. McLean, & H. Takami, 91470L, doi: [10.1117/12.2055132](https://doi.org/10.1117/12.2055132)
- de Jong, R. S., Agertz, O., Berbel, A. A., et al. 2019, *The Messenger*, 175, 3, doi: [10.18727/0722-6691/5117](https://doi.org/10.18727/0722-6691/5117)
- Espaillet, C., Patterson, J., Warner, B., & Woudt, P. 2005, *PASP*, 117, 189, doi: [10.1086/427959](https://doi.org/10.1086/427959)
- Finch, E., Bartolucci, G., Chucherko, D., et al. 2023, *MNRAS*, 522, 5358, doi: [10.1093/mnras/stad1288](https://doi.org/10.1093/mnras/stad1288)
- Fontaine, G., et al. 2011, *ApJ*, 726, 92, doi: [10.1088/0004-637X/726/2/92](https://doi.org/10.1088/0004-637X/726/2/92)
- Gaia Collaboration, Brown, A. G. A., Vallenari, A., et al. 2020, arXiv e-prints, arXiv:2012.01533, <https://arxiv.org/abs/2012.01533>
- Gaia Collaboration, Prusti, T., de Bruijne, J. H. J., et al. 2016, *A&A*, 595, A1, doi: [10.1051/0004-6361/201629272](https://doi.org/10.1051/0004-6361/201629272)
- Gaia Collaboration, Brown, A. G. A., Vallenari, A., et al. 2018, *A&A*, 616, A1, doi: [10.1051/0004-6361/201833051](https://doi.org/10.1051/0004-6361/201833051)
- Gaia Collaboration, Vallenari, A., Brown, A. G. A., et al. 2022, arXiv e-prints, arXiv:2208.00211, <https://arxiv.org/abs/2208.00211>
- Geier, S., Marsh, T. R., Wang, B., et al. 2013, *A&A*, 554, A54, doi: [10.1051/0004-6361/201321395](https://doi.org/10.1051/0004-6361/201321395)
- Green, G. M., Schlafly, E., Zucker, C., Speagle, J. S., & Finkbeiner, D. 2019, *ApJ*, 887, 93, doi: [10.3847/1538-4357/ab5362](https://doi.org/10.3847/1538-4357/ab5362)
- Green, G. M., Schlafly, E. F., Finkbeiner, D., et al. 2018, *MNRAS*, 478, 651, doi: [10.1093/mnras/sty1008](https://doi.org/10.1093/mnras/sty1008)
- Green, M. J., Hermes, J. J., Barlow, B. N., et al. 2024, *MNRAS*, 527, 3445, doi: [10.1093/mnras/stad3412](https://doi.org/10.1093/mnras/stad3412)
- Groot, P. J., Nelemans, G., Steeghs, D., & Marsh, T. R. 2001, *ApJL*, 558, L123, doi: [10.1086/323605](https://doi.org/10.1086/323605)
- Harms, J., Ambrosino, F., Angelini, L., et al. 2021, *ApJ*, 910, 1, doi: [10.3847/1538-4357/abe5a7](https://doi.org/10.3847/1538-4357/abe5a7)
- Heinze, A. N., Tonry, J. L., Denneau, L., et al. 2018, *AJ*, 156, 241, doi: [10.3847/1538-3881/aae47f](https://doi.org/10.3847/1538-3881/aae47f)
- Hermes, J. J., Kilic, M., Brown, W. R., et al. 2012, *ApJL*, 757, L21, doi: [10.1088/2041-8205/757/2/L21](https://doi.org/10.1088/2041-8205/757/2/L21)
- Howell, S. B., Szkody, P., Kreidl, T. J., & Dobrzycka, D. 1991, *PASP*, 103, 300, doi: [10.1086/132819](https://doi.org/10.1086/132819)
- Huang, S.-J., Hu, Y.-M., Korol, V., et al. 2020, *PhRvD*, 102, 063021, doi: [10.1103/PhysRevD.102.063021](https://doi.org/10.1103/PhysRevD.102.063021)
- Hunter, J. D. 2007, *Computing In Science & Engineering*, 9, 90, doi: [10.1109/MCSE.2007.55](https://doi.org/10.1109/MCSE.2007.55)
- Igoshev, A., Verbunt, F., & Cator, E. 2016, *A&A*, 591, A123, doi: [10.1051/0004-6361/201527471](https://doi.org/10.1051/0004-6361/201527471)
- Irrgang, A., Wilcox, B., Tucker, E., & Schiefelbein, L. 2013, *A&A*, 549, A137, doi: [10.1051/0004-6361/201220540](https://doi.org/10.1051/0004-6361/201220540)
- Kilic, M., Brown, W. R., Bédard, A., & Kosakowski, A. 2021, *ApJL*, 918, L14, doi: [10.3847/2041-8213/ac1e2b](https://doi.org/10.3847/2041-8213/ac1e2b)
- Kilic, M., Brown, W. R., Gianninas, A., et al. 2017, *MNRAS*, 471, 4218, doi: [10.1093/mnras/stx1886](https://doi.org/10.1093/mnras/stx1886)
- . 2014, *MNRAS*, 444, L1, doi: [10.1093/mnrasl/slu093](https://doi.org/10.1093/mnrasl/slu093)
- Kilic, M., Brown, W. R., Hermes, J. J., et al. 2011a, *MNRAS*, 418, L157, doi: [10.1111/j.1745-3933.2011.01165.x](https://doi.org/10.1111/j.1745-3933.2011.01165.x)
- Kilic, M., Brown, W. R., Kenyon, S. J., et al. 2011b, *MNRAS*, 413, L101, doi: [10.1111/j.1745-3933.2011.01044.x](https://doi.org/10.1111/j.1745-3933.2011.01044.x)
- Klein, A., Pratten, G., Buscicchio, R., et al. 2022, arXiv e-prints, arXiv:2204.03423, <https://arxiv.org/abs/2204.03423>
- Kollmeier, J. A., Zasowski, G., Rix, H.-W., et al. 2017, arXiv e-prints, arXiv:1711.03234, <https://arxiv.org/abs/1711.03234>
- Korol, V., Hallakoun, N., Toonen, S., & Karnesis, N. 2022, *MNRAS*, 511, 5936, doi: [10.1093/mnras/stac415](https://doi.org/10.1093/mnras/stac415)

- Korol, V., Igoshev, A. P., Toonen, S., et al. 2023, arXiv e-prints, arXiv:2310.06559, doi: [10.48550/arXiv.2310.06559](https://doi.org/10.48550/arXiv.2310.06559)
- Korol, V., Rossi, E. M., Groot, P. J., et al. 2017, MNRAS, 470, 1894, doi: [10.1093/mnras/stx1285](https://doi.org/10.1093/mnras/stx1285)
- Kosakowski, A., Brown, W. R., Kilic, M., et al. 2023a, ApJ, 950, 141, doi: [10.3847/1538-4357/acd187](https://doi.org/10.3847/1538-4357/acd187)
- Kosakowski, A., Kilic, M., & Brown, W. 2021, MNRAS, 500, 5098, doi: [10.1093/mnras/staa3571](https://doi.org/10.1093/mnras/staa3571)
- Kosakowski, A., Kilic, M., Brown, W. R., & Gianninas, A. 2020, ApJ, 894, 53, doi: [10.3847/1538-4357/ab8300](https://doi.org/10.3847/1538-4357/ab8300)
- Kosakowski, A., Kupfer, T., Bergeron, P., & Littenberg, T. B. 2023b, ApJ, 959, 114, doi: [10.3847/1538-4357/ad0ce9](https://doi.org/10.3847/1538-4357/ad0ce9)
- Kupfer, T., Groot, P. J., Bloemen, S., et al. 2015, MNRAS, 453, 483, doi: [10.1093/mnras/stv1609](https://doi.org/10.1093/mnras/stv1609)
- Kupfer, T., Korol, V., Shah, S., et al. 2018, MNRAS, 480, 302, doi: [10.1093/mnras/sty1545](https://doi.org/10.1093/mnras/sty1545)
- Kupfer, T., Bauer, E. B., Marsh, T. R., et al. 2020a, ApJ, 891, 45, doi: [10.3847/1538-4357/ab72ff](https://doi.org/10.3847/1538-4357/ab72ff)
- Kupfer, T., Bauer, E. B., Burdge, K. B., et al. 2020b, ApJL, 898, L25, doi: [10.3847/2041-8213/aba3c2](https://doi.org/10.3847/2041-8213/aba3c2)
- Kupfer, T., Prince, T. A., van Roestel, J., et al. 2021, MNRAS, 505, 1254, doi: [10.1093/mnras/stab1344](https://doi.org/10.1093/mnras/stab1344)
- Kupfer, T., Bauer, E. B., van Roestel, J., et al. 2022, ApJL, 925, L12, doi: [10.3847/2041-8213/ac48f1](https://doi.org/10.3847/2041-8213/ac48f1)
- Lamberts, A., Blunt, S., Littenberg, T. B., et al. 2019, MNRAS, 490, 5888, doi: [10.1093/mnras/stz2834](https://doi.org/10.1093/mnras/stz2834)
- Laureijs, R., Amiaux, J., Arduini, S., et al. 2011, arXiv e-prints, arXiv:1110.3193, doi: [10.48550/arXiv.1110.3193](https://doi.org/10.48550/arXiv.1110.3193)
- Levitan, D., Fulton, B. J., Groot, P. J., et al. 2011, ApJ, 739, 68, doi: [10.1088/0004-637X/739/2/68](https://doi.org/10.1088/0004-637X/739/2/68)
- Levitan, D., Kupfer, T., Groot, P. J., et al. 2014, ApJ, 785, 114, doi: [10.1088/0004-637X/785/2/114](https://doi.org/10.1088/0004-637X/785/2/114)
- Li, Z., Chen, X., Chen, H.-L., et al. 2020, ApJ, 893, 2, doi: [10.3847/1538-4357/ab7dc2](https://doi.org/10.3847/1538-4357/ab7dc2)
- Lindgren, L., Hernandez, J., Bombrun, A., et al. 2018, ArXiv e-prints. <https://arxiv.org/abs/1804.09366>
- LISA Science Study Team. 2018, LISA Science Requirements Document, Tech. Rep. ESA-L3-EST-SCI-RS-001, ESA. www.cosmos.esa.int/web/lisa/lisa-documents/
- Littenberg, T. B. 2018, PhRvD, 98, 043008, doi: [10.1103/PhysRevD.98.043008](https://doi.org/10.1103/PhysRevD.98.043008)
- Littenberg, T. B., & Cornish, N. J. 2019, ApJL, 881, L43, doi: [10.3847/2041-8213/ab385f](https://doi.org/10.3847/2041-8213/ab385f)
- . 2023, PhRvD, 107, 063004, doi: [10.1103/PhysRevD.107.063004](https://doi.org/10.1103/PhysRevD.107.063004)
- Littenberg, T. B., Cornish, N. J., Lackeos, K., & Robson, T. 2020, Phys. Rev. D, 101, 123021, doi: [10.1103/PhysRevD.101.123021](https://doi.org/10.1103/PhysRevD.101.123021)
- Luo, J., Chen, L.-S., Duan, H.-Z., et al. 2016, Classical and Quantum Gravity, 33, 035010, doi: [10.1088/0264-9381/33/3/035010](https://doi.org/10.1088/0264-9381/33/3/035010)
- Luri, X., Brown, A. G. A., Sarro, L. M., et al. 2018, ArXiv e-prints. <https://arxiv.org/abs/1804.09376>
- Lyne, A. G., Burgay, M., Kramer, M., et al. 2004, Science, 303, 1153, doi: [10.1126/science.1094645](https://doi.org/10.1126/science.1094645)
- Marsh, T. R. 2011, Classical and Quantum Gravity, 28, 094019, doi: [10.1088/0264-9381/28/9/094019](https://doi.org/10.1088/0264-9381/28/9/094019)
- Munday, J., Marsh, T. R., Hollands, M., et al. 2023, MNRAS, 518, 5123, doi: [10.1093/mnras/stac3385](https://doi.org/10.1093/mnras/stac3385)
- Nelemans, G., & Jonker, P. G. 2010, NewAR, 54, 87, doi: [10.1016/j.newar.2010.09.021](https://doi.org/10.1016/j.newar.2010.09.021)
- Nelemans, G., Portegies Zwart, S. F., Verbunt, F., & Yungelson, L. R. 2001, A&A, 368, 939, doi: [10.1051/0004-6361:20010049](https://doi.org/10.1051/0004-6361:20010049)
- Nelemans, G., Yungelson, L. R., & Portegies Zwart, S. F. 2004, MNRAS, 349, 181, doi: [10.1111/j.1365-2966.2004.07479.x](https://doi.org/10.1111/j.1365-2966.2004.07479.x)
- Nissanke, S., Vallisneri, M., Nelemans, G., & Prince, T. A. 2012, ApJ, 758, 131, doi: [10.1088/0004-637X/758/2/131](https://doi.org/10.1088/0004-637X/758/2/131)
- Oliphant, T. E. 2015, Guide to NumPy, 2nd edn. (USA: CreateSpace Independent Publishing Platform)
- Patterson, J., Fried, R. E., Rea, R., et al. 2002, PASP, 114, 65, doi: [10.1086/339450](https://doi.org/10.1086/339450)
- Pauli, E. M., Napiwotzki, R., Altmann, M., et al. 2003, A&A, 400, 877, doi: [10.1051/0004-6361:20030012](https://doi.org/10.1051/0004-6361:20030012)
- Pauli, E.-M., Napiwotzki, R., Heber, U., Altmann, M., & Odenkirchen, M. 2006, A&A, 447, 173, doi: [10.1051/0004-6361:20052730](https://doi.org/10.1051/0004-6361:20052730)
- Pelisoli, I., Neunteufel, P., Geier, S., et al. 2021, Nature Astronomy, 5, 1052, doi: [10.1038/s41550-021-01413-0](https://doi.org/10.1038/s41550-021-01413-0)
- Penoyre, Z., Belokurov, V., Wyn Evans, N., Everall, A., & Koposov, S. E. 2020, MNRAS, 495, 321, doi: [10.1093/mnras/staa114810.48550/arXiv.2003.05456](https://doi.org/10.1093/mnras/staa114810.48550/arXiv.2003.05456)
- Petiteau, A. 2008, Theses, Université Paris-Diderot - Paris VII. <https://theses.hal.science/tel-00383222>
- Provencal, J. L., Winget, D. E., Nather, R. E., et al. 1997, ApJ, 480, 383, doi: [10.1086/303971](https://doi.org/10.1086/303971)
- Ramsay, G., Hakala, P., & Cropper, M. 2002, MNRAS, 332, L7, doi: [10.1046/j.1365-8711.2002.05471.x](https://doi.org/10.1046/j.1365-8711.2002.05471.x)
- Ramsay, G., Green, M. J., Marsh, T. R., et al. 2018, A&A, 620, A141, doi: [10.1051/0004-6361/201834261](https://doi.org/10.1051/0004-6361/201834261)
- Reinsch, K., Steiper, J., & Dreizler, S. 2007, in Astronomical Society of the Pacific Conference Series, Vol. 372, 15th European Workshop on White Dwarfs, ed. R. Napiwotzki & M. R. Burleigh, 419

- Roebber, E., Buscicchio, R., Vecchio, A., et al. 2020, *ApJL*, 894, L15, doi: [10.3847/2041-8213/ab8ac9](https://doi.org/10.3847/2041-8213/ab8ac9)
- Roelofs, G. H. A., Groot, P. J., Benedict, G. F., et al. 2007, *ApJ*, 666, 1174, doi: [10.1086/520491](https://doi.org/10.1086/520491)
- Roelofs, G. H. A., Groot, P. J., Marsh, T. R., Steeghs, D., & Nelemans, G. 2006, *MNRAS*, 365, 1109, doi: [10.1111/j.1365-2966.2005.09727.x](https://doi.org/10.1111/j.1365-2966.2005.09727.x)
- Roelofs, G. H. A., Rau, A., Marsh, T. R., et al. 2010, *ApJL*, 711, L138, doi: [10.1088/2041-8205/711/2/L138](https://doi.org/10.1088/2041-8205/711/2/L138)
- Ruan, W.-H., Guo, Z.-K., Cai, R.-G., & Zhang, Y.-Z. 2018, arXiv e-prints, arXiv:1807.09495. <https://arxiv.org/abs/1807.09495>
- Ruiter, A. J., Belczynski, K., Benacquista, M., & Holley-Bockelmann, K. 2009, *ApJ*, 693, 383, doi: [10.1088/0004-637X/693/1/383](https://doi.org/10.1088/0004-637X/693/1/383)
- Savalle, E., Gair, J., Speri, L., & Babak, S. 2022, *PhRvD*, 106, 022003, doi: [10.1103/PhysRevD.106.022003](https://doi.org/10.1103/PhysRevD.106.022003)
- Scaringi, S., Breivik, K., Littenberg, T. B., et al. 2023, *MNRAS*, 525, L50, doi: [10.1093/mnras/525/1/L50](https://doi.org/10.1093/mnras/525/1/L50)
- Shah, S., & Nelemans, G. 2014, *ApJ*, 790, 161, doi: [10.1088/0004-637X/790/2/161](https://doi.org/10.1088/0004-637X/790/2/161)
- Shah, S., van der Sluys, M., & Nelemans, G. 2012, *A&A*, 544, A153, doi: [10.1051/0004-6361/201219309](https://doi.org/10.1051/0004-6361/201219309)
- Skillman, D. R., Patterson, J., Kemp, J., et al. 1999, *PASP*, 111, 1281, doi: [10.1086/316437](https://doi.org/10.1086/316437)
- Solheim, J. E. 2010, *Publications of the Astronomical Society of the Pacific*, 122, 1133, doi: [10.1086/656680](https://doi.org/10.1086/656680)
- Steeghs, D., Marsh, T. R., Barros, S. C. C., et al. 2006, *ApJ*, 649, 382, doi: [10.1086/506343](https://doi.org/10.1086/506343)
- Steeghs, D., Galloway, D. K., Ackley, K., et al. 2022, *MNRAS*, 511, 2405, doi: [10.1093/mnras/stac013](https://doi.org/10.1093/mnras/stac013)
- Stella, L., Priedhorsky, W., & White, N. E. 1987, *ApJL*, 312, L17, doi: [10.1086/184811](https://doi.org/10.1086/184811)
- Ströer, A., & Vecchio, A. 2006, *Classical and Quantum Gravity*, 23, 809, doi: [10.1088/0264-9381/23/19/S19](https://doi.org/10.1088/0264-9381/23/19/S19)
- Strohmayer, T. E. 2005, *ApJ*, 627, 920, doi: [10.1086/430439](https://doi.org/10.1086/430439)
- Szekerczes, K., Noble, S., Chirenti, C., & Thorpe, J. I. 2023, *AJ*, 166, 17, doi: [10.3847/1538-3881/acd3f1](https://doi.org/10.3847/1538-3881/acd3f1)
- Tauris, T. M. 2018, *PhRvL*, 121, 131105, doi: [10.1103/PhysRevLett.121.131105](https://doi.org/10.1103/PhysRevLett.121.131105)
- Tonry, J. L., Denneau, L., Heinze, A. N., et al. 2018, *PASP*, 130, 064505, doi: [10.1088/1538-3873/aabadf](https://doi.org/10.1088/1538-3873/aabadf)
- van Paradijs, J., & McClintock, J. E. 1994, *A&A*, 290, 133
- van Roestel, J., Kupfer, T., Green, M. J., et al. 2022, *MNRAS*, 512, 5440, doi: [10.1093/mnras/stab2421](https://doi.org/10.1093/mnras/stab2421)
- Wevers, T., Torres, M. A. P., Jonker, P. G., et al. 2016, *MNRAS*, 462, L106, doi: [10.1093/mnras/462/1/L106](https://doi.org/10.1093/mnras/462/1/L106)
- Wilhelm, M. J. C., Korol, V., Rossi, E. M., & D'Onghia, E. 2021, *MNRAS*, 500, 4958, doi: [10.1093/mnras/staa3457](https://doi.org/10.1093/mnras/staa3457)
- Wood, M. A., Casey, M. J., Garnavich, P. M., & Haag, B. 2002, *MNRAS*, 334, 87, doi: [10.1046/j.1365-8711.2002.05484.x](https://doi.org/10.1046/j.1365-8711.2002.05484.x)
- Zhao, G., Zhao, Y., Chu, Y., Jing, Y., & Deng, L. 2012, arXiv e-prints, arXiv:1206.3569, doi: [10.48550/arXiv.1206.3569](https://doi.org/10.48550/arXiv.1206.3569)